Light stop/sbottom pair production searches in the NMSSM

Xiao-Jun Bi[1], Qi-Shu Yan[2], and Peng-Fei Yin[1]

[1]*Laboratory of Particle Astrophysics, Institute of High Energy Physics, Chinese Academy of Sciences, Beijing 100049, China and*

[2]*College of Physics Sciences, University of Chinese Academy of Sciences, Beijing 100049, China*

In this work, we study the constraints on the scenario of light stop and sbottom in the next-to-minimal supersymmetric standard model (NMSSM), especially by a 125 GeV Higgs boson discovery and the LHC bounds on supersymmetry. The constraints from dark matter detections are also taken into account. From the parameter scan, we find that the NMSSM can accommodate a light Higgs boson around 125 GeV and decay patterns well. The LHC direct SUSY searches with b-tagging are very powerful and can set strong bounds on many NMSSM parameter points with light stop and sbottom. We find $\tilde{t} \to b\tilde{\chi}_1^+$ is a very promising channel for light stop detection if the mass splitting between $\tilde{\chi}_1^+$ and $\tilde{\chi}_1^0$ is very small. It is also pointed out that in order to close the parameter space of light stop and sbottom, new search strategies for signal channels such as $pp \to \tilde{t}_1\tilde{t}_1 \to t\bar{t}hh\tilde{\chi}_1^0\tilde{\chi}_1^0$ and $pp \to \tilde{b}_1\tilde{b}_1 \to t\bar{t}W^+W^-\tilde{\chi}_1^0\tilde{\chi}_1^0$ may be necessary.

PACS numbers: 12.60.Jv,14.80.Ly

I. INTRODUCTION

The searches from ATLAS [1], CMS [2], and CDF [3] as well as D0 [4] established that there is a new particle around $125 \sim 127$ GeV, of which its decay pattern is consistent with the predicted Higgs boson of the standard model (SM). If this new particle is a fundamental Higgs boson, it is reasonable to ask whether it is the predicted light CP-even Higgs boson in the supersymmetric models. However, a Higgs boson of 125 GeV seems a bit heavy for the minimal supersymmetric standard model (MSSM). In the MSSM, the tree-level mass of the lighter CP-even Higgs boson should always be smaller than the mass of Z boson, while the loop effects of stop can lift the Higgs boson mass up to 130 GeV or so. In order to avoid fine tuning problem, natural supersymmetry requires the third generation squarks are light

[5, 6].

Compared with the MSSM, a Higgs boson at 125 GeV can be realized more naturally in the NMSSM without confronting with the severe fine tuning problem, since it can have a much larger tree-level Higgs mass. This might be one of the reasons why NMSSM is appealing except that it solves the notorious μ problem in the MSSM. In Ref. [7], the authors studied the constrained NMSSM with all parameters defined at the grand unification scale. It is found that the tension of the constrained MSSM for a 125 GeV Higgs boson mass and a light SUSY mass spectrum can be relaxed in NMSSM with more general parameters.

Another reason that may favor NMSSM is the Higgs decay mode. The experimental data of the Higgs boson decay modes has shown a possible excess in the diphoton channel. It may be a hint of new physics [8–10]. In Ref. [11, 12], it is shown that the NMSSM can accommodate the 125 GeV Higgs and enhance the branching of fraction $BR(h \to \gamma\gamma)$ by reducing the branching fraction of $BR(h \to b\bar{b})$ via mixing effect. A comprehensive study considering light third generation sparticles in the NMSSM also found the diphoton decay branching fraction can be enhanced [13]. Moreover, light charged sparticles such as charginos and charged Higgs boson may also contribute to the Higgs diphoton decay channel significantly [14]. More studies on diphoton enhancement in both MSSM and NMSSM context can be found in [8, 15–20].

LHC is searching for SUSY particles extensively in various channels. Up to now the null-result puts tension to many SUSY models. In Ref. [21] it is found that the LHC sparticle search with 1 fb^{-1} at $\sqrt{s} = 7$ TeV exacerbated the tension between the $\delta(g-2)_\mu^{\rm SUSY}$ anomaly and the branching fraction $BR(B \to X_s\gamma)$ in the constrained minimal supersymmetric standard model (CMSSM). Of course, such conclusion is based on the assumed GUT relations among the soft breaking terms. When such relations are released as demonstrated in [22], the conclusion can be relaxed. For the pMSSM with 19-dimensional parameter space the current LHC search can not put very restrict constraints on supersymmetry in general.

The LHC direct SUSY searches have set strong constraints on the masses of gluino and first two generations of squarks in mSUGAR and some simplified models [23, 24]. Recently, there are many works on detection of light third generation squarks and gluino below 1 TeV. It is pointed out that if the stop is light its signature is possibly hidden from the LHC searches and can avoid severe LHC constraints [6, 25–27]. Therefore the natural SUSY scenario is still alive. More studies [28–35] are trying to improve the sensitivity of light stop

searches. For example, in [29, 30], the authors considered the stop dileptonic final state and explored a few kinematic observables to distinguish signal and background. The authors of Ref. [31] studied the top tagging technique for the stop search with semi-leptonic and dileptonic modes at the LHC. The hadronic top tagging technique has been examined in Ref. [32]. Interesting multiple lepton and jet final states from the multiple top decays are investigated in [36]. Moreover, light sbottom searches are investigated in [37–39]. Especially the sbottom-neutralino coannihilation scenario has been considered, it is found LHC has a good sensitivity to the parameter space by using tagged b-jet even for small mass splitting between sbottom and neutralino.

Since in the NMSSM light stop and sbottom can be natural for a 125 GeV Higgs boson [12, 13], we did a systematic study to investigate the constraints on such a light stop/sbottom scenario from the LHC SUSY searches in this work. The constraints from B physics measurements and dark matter detections as well as the Higgs boson mass on the NMSSM parameter space are first considered. Then we study the constraints from various SUSY search channels at the LHC with $\sqrt{s} = 7$ TeV and $2 \sim 5$ fb^{-1} of data, including the jets + MET channel, associated monojet channel, lepton + jets + MET channel with and without tagged b jet(s). Since both stop and sbottom can decay into b jets, it is expected that b tagging should play an important role to distinguish signal and background. Our results confirm this point and find the direct SUSY searches are powerful to exclude many parameter points with light stop and sbottom up to 500 GeV.

The paper is organized as follows. In Section II, we briefly describe the NMSSM and our parameter scanning strategy. We will concentrate on the contribution of light stop to the mass of the discovered 125 GeV Higgs boson and the constraints from dark matter searches on the neutralino sector. In Section III, we analyze the LHC bounds from both ATLAS and CMS collaborations on the signatures of the light stop pair and sbottom pair production. Section IV is the discussions and conclusions.

II. THE NMSSM

In the NMSSM a singlet superfield S is introduced to solve the so-called "μ problem". The superpotential of NMSSM related to this singlet superfield S is given by [40]:

$$W_{NMSSM} = \lambda \hat{S} \hat{H}_u \hat{H}_d + \frac{1}{3} \kappa \hat{S}^3 + ..., \tag{1}$$

where the dots denote the MSSM superpotential without μ term. When the electroweak symmetry is broken, the effective μ term can be naturally generated via the vacuum expectation value of S filed (labeled as v_S), and can be written as $\mu_{eff} = \lambda v_S$, which is expected to be of $\mathcal{O}(100)$ GeV (of the same size as the rest of soft breaking terms). This μ_{eff} can be traded off with m_S^2, the mass parameter of the superfield S. The soft-breaking terms in the Higgs sector [40] is extended as

$$V_{NMSSM} = \tilde{m}_{H_u}^2|H_u|^2 + \tilde{m}_{H_d}^2|H_d|^2 + \tilde{m}_S^2|S|^2 + (A_\lambda \lambda S H_u H_d + \frac{1}{3}A_\kappa \kappa S^3) + h.c. \quad (2)$$

Compared with the MSSM, the Higgs sector becomes richer and contains three CP-even Higgs bosons, *i.e.* H_1, H_2, and H_3, and two CP-odd Higgs bosons, *i.e.* A_1 and A_2. Five new parameters λ, κ, A_λ, A_κ and μ_{eff} are added compared with the MSSM.

A. The Parameter space

We use NMSSMTools [41] to perform a scan over the parameter space of the NMSSM. To obtain more generic conclusions, we consider the parameters defined at the electro-weak scale in our scan without assuming the unification of the NMSSM parameters at the GUT scale. We vary them in the ranges defined below:

$$\begin{aligned}
&10^{-4} < \kappa < 0.5, \quad 1 < \tan\beta < 60, \quad 50 < \mu < 500\text{GeV}, \\
&|A_\lambda| < 4\text{TeV}, \quad |A_\kappa| < 500\text{GeV}, \quad 10\text{GeV} < M_1 < 1\text{TeV}, 100\text{GeV} < M_2 < 1\text{TeV}, \\
&100\text{GeV} < m_{Q_3}, m_{U_3} < 2\text{TeV}, \quad |A_{U_3}| < 3\text{TeV}, \quad 100\text{GeV} < m_{\tilde{l}} < 1\text{TeV}. \qquad (3)
\end{aligned}$$

There are a few comments in order on the ranges of NMSSM parameters.

- The large λ is helpful to raise the SM-like Higgs mass at tree-level and to ameliorate the fine-tuning issue confronted by the MSSM. When λ tends to be zero, the singlet S will decouple from other Higgs fields. Under this limit, the phenomenology of the NMSSM may still be different from the MSSM due to the light singlet and singlino. These particles could affect the features of dark matter (DM). The decay modes of heavy sparticles produced at the colliders may also change, and some new search strategies will be necessary. Therefore we adopt two scan strategies which allow λ varies in the ranges of $[10^{-3}, 0.1]$ and $[0.1, 0.8]$ with logarithmic and flat distribution respectively.

- For the gluino and the first two generations of squarks, if their decay products are energetic jets and large MET can be reconstructed, the recent LHC results can put stringent limits on their masses in mSURGA and phenomenological SUSY, e.g. $M_3 \sim m_{\tilde{q}_{1,2}} > 1.4\text{TeV}$ [23]. If the first two generations of squarks are very heavy, the SUSY flavor and CP problems can be solved [42]. For the gluino, the naturalness of Higgs mass requires its mass should not be much larger than $\sim 1\text{TeV}$ [6]. The main decay mode of gluino may be $\tilde{g} \to t\tilde{t}/b\tilde{b}$. For simplicity, in this work, we focus on the pair production of the third generation of squarks and leave this case for future study. Therefore we fix the soft-breaking parameters $M_3 = m_{\tilde{q}_{1,2}} = 1.5\text{TeV}$. To reduce the number of free parameters, we also assume the mass parameters of the third generation of right-handed squarks are the same, *i.e.* $m_{D_3} = m_{U_3}$.

- In our scan, we require the mass of SM-like Higgs is in the range of $125 \pm 2\text{GeV}$ and the SM-like Higgs boson can be either H_1 or H_2. Except this, several phenomenology and astrophysics experimental limits are also considered. For flavor constraints, we require $\text{BR}(B_s \to X_s\gamma)$, $\text{BR}(B^+ \to \tau^+\nu_\tau)$, $\text{BR}(B \to X_s\mu^+\mu^-)$, ΔM_d and ΔM_s satisfying experimental constraints at 2σ [43–45]. The theoretical uncertainties in these observables are considered as implemented in NMSSMTools. For $\text{BR}(B_s \to \mu^+\mu^-)$, the upper-limits have evolved much in these two years. Recently ATLAS, CMS and LHCb collaborations have updated it to 2.2×10^{-8} [46], 7.7×10^{-9} [47] and 4.5×10^{-9} [48] at 95% confidence level, respectively, which are only a few times above the SM predictions. Here we adopt constraint $\text{BR}(B_s \to \mu^+\mu^-) < 4.5 \times 10^{-9}$ given by LHCb. For the muon anomalous magnetic moment α_μ, we require SUSY effects can explain the discrepancy between SM prediction and experimental result at 2σ. The mass limits for Higgs and charged SUSY particles from LEP, Tevatron and early LHC data are also adopted by in the NMSSMTools package [41].

- In our analysis, the lightest neutralino is required to be LSP and a candidate of the DM. Considering that there may be several types of DM in our universe, then the LSP in the NMSSM is just one kind of the DM, We only require the thermal abundance of neutralino satisfies a 3σ upper-limit $\Omega_\chi h^2 < 0.1288$ with the corrected DM relic density $\Omega h^2 = 0.112 \pm 0.0056$ reported by the WMAP [49]. For this purpose, we define a fraction variable $\xi = \Omega_\chi h^2/\Omega h^2$, and the neutralino density in halo is $\rho_\chi = \xi\rho_{DM}$. The

DM detection limits given by experimental collaborations are obtained by assuming a certain DM density $\rho_{DM} \sim 0.3$ GeV cm^{-3}. Thus for the parameter points predicting $\Omega_\chi h^2 \ll \Omega h^2$, these limits need to be rescaled. By doing this, we can examine whether the LSP in the NMSSM can sufficiently accommodate all data. The dark matter observations are calculated by MicrOmega [50] implemented in the NMSSMTools.

Because this numerical scan is performed over a multi-dimensional parameter space, we use a Markov Chain Monte-Carlo (MCMC) method to increase the scan efficiency in our analysis. The total likelihood function $L_{tot} = \Pi_i L_i$ is evaluated by the likelihood functions based on the phenomenology and astrophysics experimental observables described above. We define $L_i = e^{-\frac{(x_i-\mu_i)^2}{2\sigma_i^2}}$ for two-sided constraints and $L_i = 1/(1+e^{\frac{x_i-\mu_i}{\sigma_i'}})$ for upper-limits [51], where x_i is the observable predicted by the model, $\mu_i \pm \sigma_i$ is the central values and error bars of experimental observables, σ' taken as $\sigma' = 0.02\mu_i$ is the tolerance for upper-limit.

B. 125GeV Higgs Boson

In the MSSM, the tree level SM-like Higgs mass is smaller than M_Z which is below the LEP limit $m_h < 114$ GeV. However, it can be lifted by the loop corrections (say top-stop corrections due the large Yukawa couplings). One loop formula for m_h is given by

$$\begin{aligned} m_h^2 &= m_{h,tree}^2 + \Delta m_{h,loop}^2 \\ &= M_Z^2 \cos^2 2\beta + \frac{3m_t^4}{4\pi^2 v^2}\left(\ln\left(\frac{M_{\tilde{t}}^2}{m_t^2}\right) + \frac{X_t^2}{M_{\tilde{t}}^2}\left(1 - \frac{X_t^2}{12M_{\tilde{t}}^2}\right)\right), \end{aligned} \tag{4}$$

where $v = 174$ is the vacuum expectation value of SM Higgs, $M_{\tilde{t}} = \sqrt{m_{\tilde{t}_1} m_{\tilde{t}_2}}$ is related to the stop masses, $X_t \equiv A_t - \mu \cot\beta$ is the stop mixing parameter. The Higgs mass depends on stop masses logarithmically. It means the stop bosons should be heavy in order to produce a large enough correction to the mass of the Higgs boson. We can also see the Higgs mass depends on stop mixing and is maximal for $X = X_t/M_{\tilde{t}} = \sqrt{6}$.

In the NMSSM, the superpotential $\lambda \hat{S}\hat{H}_u\hat{H}_d$ can induce a new term $\lambda^2 v^2 \sin 2\beta H_u H_d$ in the Higgs potential. After rotating the 2×2 mass matrix of two CP-even neutral Higgs of doublets H_U and H_D by angle β, one diagonal element becomes $M_Z^2 \cos^2 2\beta + \lambda^2 v^2 \sin^2 2\beta$, which means that compared with the MSSM, the SM-like Higgs mass (mainly H_U type Higgs boson) obtains a new contribution $\sim \lambda^2 \sin^2 2\beta$ [40]:

$$m_h^2 = M_Z^2 \cos^2 2\beta + \lambda^2 v^2 \sin^2 2\beta + \Delta m_{h,loop}^2 + ..., \tag{5}$$

where dots denote the effects from mixing between Higgs doublets and the singlet. For large λ with $\lambda v > M_Z$, the m_h is maximized for $\tan\beta = 1$. Note that even $\sin 2\beta = 1$ and λ is taken as its maximal value ~ 0.7 which is consistent with the perturbation condition at the GUT scale, we still need a moderate stop loop contribution to obtain a 125 GeV Higgs.

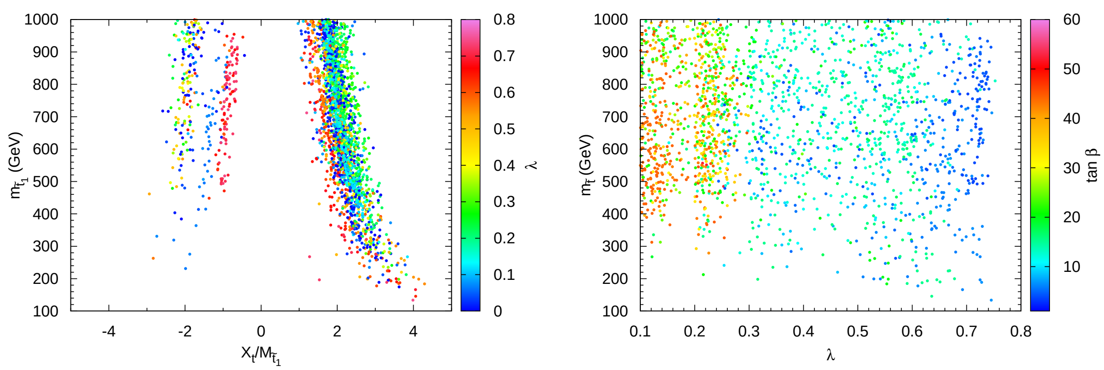

FIG. 1: Left: $m_{\tilde{t}_1}$ versus $X_t/M_{\tilde{t}}$. Right: $m_{\tilde{t}_1}$ versus λ. The color scale indicates λ (left) and $\tan\beta$ (right) respectively.

It is interesting to ask how light the stop can reach after taking into account the 125 GeV Higgs boson in the NMSSM. To address such a question, below we show some scattering plots. In these plots, all the points have passed the constraints as being described in Sec. II A.

In the left panel of Fig. (1), we show the correlation in the $m_{\tilde{t}_1} - X$ plane, the color bar shows the value of λ. It is observed that for the large $\lambda \sim 0.6 - 0.7$, the stop mixing parameter $|X|$ is allowed to be 1. When the light stop mass decreases, the stop mixing parameter will increase. If $m_{\tilde{t}_1}$ is below 300 GeV, X should be large than 3. It means there is a large mass splitting between two stop states. Because λ can raise the mass of Higgs boson efficiently, it is easier to obtain a lighter $\tilde{t}_1$ with a larger λ.

In the right panel of Fig. (1), we show the correlations between $m_{\tilde{t}_1}$ and λ, the color scale indicates $\tan\beta$. We also see that there are many points with small $m_{\tilde{t}_1}$ in the large λ regime. As shown in Eq. 5, the Higgs mass depends on $\lambda \sin 2\beta$, the values of $\tan\beta$ decrease at large λ. We can see $\tan\beta < 30$ for $\lambda > 0.3$ and $\tan\beta < 10$ for $\lambda > 0.6$.

Another interesting question is whether the NMSSM can accommodate the decay modes

and the decay branching fractions measured by the LHC collaborations appropriately. Especially whether the NMSSM can explain the diphoton excesses and diboson (mainly $h \to ZZ$) data observed by LHC collaborations? Below we address this issue.

In the SM, if the Higgs mass is determined, all the Higgs interaction couplings to SM particles can be obtained. In the new physics model, the Higgs couplings may differ to the SM predictions due to new parameters and particles. Therefore, the searches of Higgs partial widths at the LHC are very important to test the SM, and can provide crucial evidences of new physics.

The effective Higgs couplings can be extracted from experimental data and can be compared with theoretical predictions. The parameter described the modifications of the Higgs couplings is defined as

$$C_{hXX} \equiv \bar{C}^{NP}_{hXX}/\bar{C}^{SM}_{hXX}, \tag{6}$$

where X can denote either heavy fermions, W boson, Z boson, photon or gluon. In the new physics model, both the production cross section and decay width of Higgs are rescaled by C_h^2. The relevant Higgs partial widths would be determined by the ratio

$$R_{hXX} = \frac{\sigma(pp \to h)_{NP} BR(h \to XX)_{NP}}{\sigma(pp \to h)_{SM} BR(h \to XX)_{SM}}. \tag{7}$$

For the $\gamma\gamma$, W^+W^- and ZZ channel, the recorded Higgs events are mainly from gluon fusion $gg \to h$ process. If the decay channel of 125 GeV Higgs is dominated by $h \to b\bar{b}$, the R_{hXX} ($X = W, Z, \gamma$) is approximated to be $R_{hXX} \sim C^2_{hgg} BR(h \to XX)_{NP}/BR(h \to XX)_{SM} \sim C^2_{hgg} C^2_{hXX}/C^2_{hb\bar{b}}$. For the $b\bar{b}$ channel, additional electrons or muons are required to suppress huge QCD background, only the electroweak production channel $q\bar{q} \to hV$ is used to search Higgs signal. Therefore, the R_{hXX} can be given by $R_{hb\bar{b}} \sim C^2_{hVV} BR(h \to b\bar{b})_{NP}/BR(h \to b\bar{b})_{SM}$.

In the NMSSM, the Higgs mass basis $H_i^{mass} = \{H_1, H_2, H_3\}$ and interaction basis $H_a^{int} = \{H_d, H_u, S\}$ are related by $H_i^{mass} = S_{ia} H_a^{int}$. The reduced Higgs couplings to fermions and heavy gauge bosons can be given by

$$C_{hb\bar{b}} = C_{h\tau\bar{\tau}} = \frac{S_{i1}}{\cos\beta}, \quad C_{ht\bar{t}} = \frac{S_{i2}}{\sin\beta}, \quad C_{hVV} = S_{i1}\cos\beta + S_{i2}\sin\beta. \tag{8}$$

In the SM, effective Higgs coupling to gluon C_{hgg} is dominantly determined by triangle top loop. In the SUSY model, stop loop would also contribute to C_{hgg}, it can be written as

$$C_{hgg} = \frac{\bar{C}^{SUSY}_{hgg,\,t} + \bar{C}^{SUSY}_{hgg,\,\tilde{t}}}{\bar{C}^{SM}_{hgg,\,t}} \sim C_{ht\bar{t}} + C_{\tilde{t}}, \tag{9}$$

where $\bar{C}_{hXX,\,A}$ is the loop contribution from particle A to the effective Higgs coupling C_{hXX}, and $C_{\tilde{t}}$ is defined as $C_{\tilde{t}} = \bar{C}^{SUSY}_{hgg,\,\tilde{t}}/\bar{C}^{SM}_{hgg,\,t}$.

For the $C_{h\gamma\gamma}$, the main contributions arise from W loop and top loop, which are related by $\bar{C}^{SM}_{h\gamma\gamma,\,W}/\bar{C}^{SM}_{h\gamma\gamma,\,t} \sim -8.3/1.8$ in the SM. In the SUSY model, light charged particles [15], such as light chargino, light charged Higgs boson, stop, sbottom, and stau, would provide additional contributions. We can also get $C_{h\gamma\gamma}$ approximately

$$C_{h\gamma\gamma} = \frac{\bar{C}^{SUSY}_{h\gamma\gamma,\,t} + \bar{C}^{SUSY}_{h\gamma\gamma,\,W} + \bar{C}^{SUSY}_{h\gamma\gamma}}{\bar{C}^{SM}_{h\gamma\gamma,\,t} + \bar{C}^{SM}_{h\gamma\gamma,\,W}} \sim 1.28C_{hVV} - 0.28(C_{ht\bar{t}} + C_{\tilde{t}}) + C_{\tilde{\tau}} + C_{\tilde{\chi}^+}, \tag{10}$$

where we have used the relations $\bar{C}^{SUSY}_{h\gamma\gamma,\,W}/\bar{C}^{SM}_{h\gamma\gamma,\,W} \sim C_{hVV}$, $\bar{C}^{SUSY}_{h\gamma\gamma,\,t}/\bar{C}^{SM}_{h\gamma\gamma,\,t} \sim C_{ht\bar{t}}$ and $\bar{C}^{SUSY}_{h\gamma\gamma,\,\tilde{t}}/\bar{C}^{SM}_{h\gamma\gamma,\,\tilde{t}} \sim \bar{C}^{SUSY}_{hgg,\,t}/\bar{C}^{SM}_{hgg,\,t}$ (neglecting the high order QCD corrections induced by stop), and $C_{\tilde{\tau}}$ is defined as $C_{\tilde{\tau}} = \bar{C}^{SUSY}_{hgg,\,\tilde{\tau}}/\bar{C}^{SM}_{h\gamma\gamma}$. Note that $C_{\tilde{\tau}}$ is proportional to Yukawa coupling $y_{h\tau\bar{\tau}}$ and inversely proportional to stau mass m_τ, it means $C_{\tilde{\tau}}$ is important for large $\tan\beta > 50 \sim 60$ and light stau [8].

An important feature of Higgs phenomenology in the NMSSM is the exotic Higgs decay modes to light neutralinos or scalars [52, 53]. If H_1 is SM-like, H_2 might be much heavier than 125 GeV. If H_2 is SM-like, H_1 and A_1 would be light singlets. In this case, the branching ratios of $H_2 \to \tilde{\chi}^0_1\tilde{\chi}^0_1$, $H_2 \to H_1H_1$ and $H_2 \to A_1A_1$ could be large due to Higgs mixing and kinematics. For the invisible Higgs decay $H_2 \to \tilde{\chi}^0_1\tilde{\chi}^0_1$, the possible search channels are $f\bar{f} \to Vh \to$ leptons+MET or $gg \to hj \to$ mono-jet+MET. For the decay channels $H_2 \to H_1H_1$ and $H_2 \to A_1A_1$, the light singlets would decay into $\tau\bar{\tau}$ or $b\bar{b}$. The final states are four fermions which can be significant for some parameter points. However, these exotic decay modes might suppress the standard Higgs decay modes to heavy gauge bosons, photons and $b\bar{b}$, and could be tested by the global-fitting of Higgs decay partial widths in the future.

To examine the question whether the NMSSM can accommodate the diphoton excess, we show scattering plots to demonstrate the correlations between the effective couplings and $R_{\gamma\gamma}$. In the left/middle/right panel of Fig. (2), we demonstrate the correlations between $R_{\gamma\gamma}$ with $C_{hb\bar{b}}/C_{h\gamma\gamma}/C_{hgg}$, the blue/red points denote SM-like Higgs is H_1/H_2. We can see $C_{h\gamma\gamma}$ and C_{hgg} always vary in the range of $\sim 0.8 - 1.1$, and $R_{\gamma\gamma}$ is sensitive to $C_{hb\bar{b}}$. We also find $R_{\gamma\gamma}$ is inversely proportional to $R_{b\bar{b}}$ and $R_{b\bar{b}}$ is larger than 1 for $R_{\gamma\gamma} > 1$.

These results can be understood in term of explanation given above. In the decoupling limit $M_A \gg M_Z$ ($M_A =$ is the mass of heavy CP-odd Higgs), the main component of SM-like

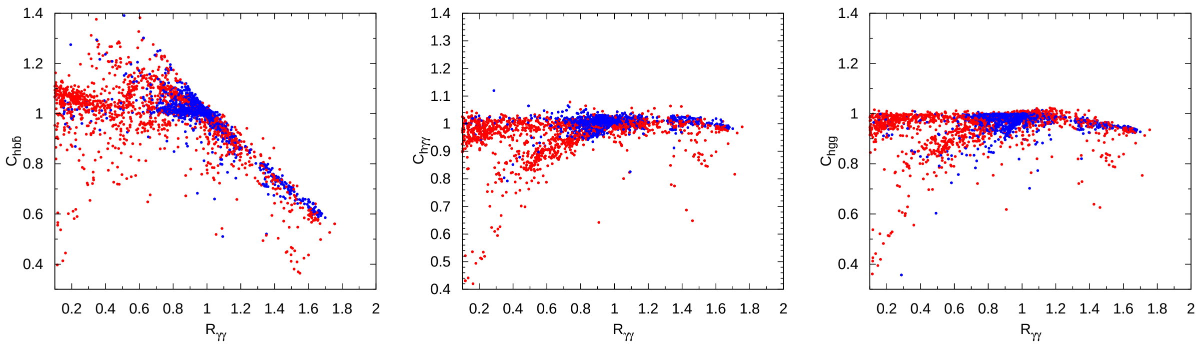

FIG. 2: The correlations between $R_{\gamma\gamma}$ and $C_{hb\bar{b}}/C_{h\gamma\gamma}/C_{hgg}$ are demonstrated. The blue/red points correspond to H_1/H_2 is the SM-like Higgs boson.

Higgs is H_u due to $S_{i2} \sim \sin\beta \sim 1$ for $\tan\beta \gg 1$. From Eq. (8), we can get $C_{ht\bar{t}}$ and C_{hWW}. If the stop mass parameter $\sqrt{m_{\tilde{t}_1} m_{\tilde{t}_2}}$ is much larger than m_t, the stop loop would not provide larger contributions to C_{hgg}. Then $C_{hgg} \sim 1$ and $C_{h\gamma\gamma} \sim 1$ can be obtained from Eq. (9) and (10) respectively. Depending on parameters in Higgs sector, $C_{hb\bar{b}}$ can be significant reduced by mixing effect. As we have mentioned, if the main SM-like Higgs decay mode is $h \to b\bar{b}$, and $R_{hXX}(X = W, Z, \gamma)$ is approximately to be $R_{hXX} \sim C^2_{hgg} C^2_{hXX}/C^2_{hb\bar{b}} \sim 1/C^2_{hb\bar{b}}$. This relation explains the inversely proportional correlation between $R_{\gamma\gamma}$ and $C_{hb\bar{b}}$ for $R_{\gamma\gamma} > 0.8$ as shown in Fig. (2). This is the case for H_1 is SM-like Higgs.

If H_2 is SM-like, the branching ratios of exotic decay modes might be significant, the $R_{\gamma\gamma}$ would be much suppressed even the $C_{hb\bar{b}}$ is still ~ 1. For either blue/red points, to decrease $R_{b\bar{b}}$ and increase $R_{\gamma\gamma}$ can be done by tuning the singlet-doublet mixing parameters.

We also show the correlations between $R_{\gamma\gamma}$ and R_{VV} in Fig. (3), the color bar indicates $C_{hb\bar{b}}$ ($R_{b\bar{b}}$) in the left (right) panel of Fig. (3). From the left panel, we can also see the $R_{b\bar{b}}$ is smaller than 1 for $R_{\gamma\gamma} > 1$. Moreover, the $R_{\gamma\gamma}$ is always proportional to R_{VV} due to the approximations $R_{hVV}/R_{\gamma\gamma} \sim C^2_{hVV}/C^2_{h\gamma\gamma}$ and $C_{\gamma\gamma} \sim 1.28 C_{VV} - 0.28 C_{t\bar{t}} + C_{SUSY}$. As we have mentioned above, $R_{hb\bar{b}}$ depends on C_{VV} due to the production process. As C_{VV} is almost $\sim 0.8 \sim 1.1$ shown in Fig. (2), $R_{hb\bar{b}}$ is mainly determined by BR($h \to b\bar{b}$). For the large $R_{\gamma\gamma} > 1$, BR($h \to b\bar{b}$) is suppressed due to small $C_{hb\bar{b}}$. We also find the $R_{\gamma\gamma}$ can be smaller than 0.5 due to the significant Higgs exotic decays, both the R_{VV} and $R_{b\bar{b}}$ are suppressed in this case too.

According to the analysis given by CMS group, the ratio of the couplings of Higgs to

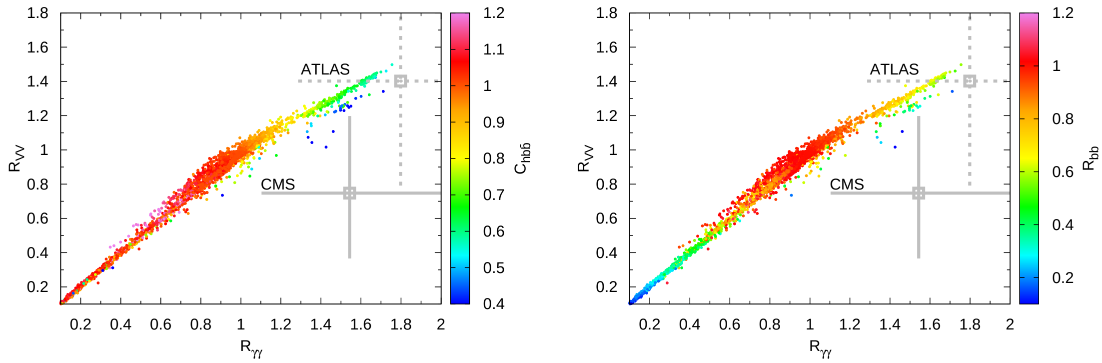

FIG. 3: The correlations between R_{VV}, $R_{\gamma\gamma}$ and $C_{b\bar{b}}/R_{b\bar{b}}$ are displayed in the left/right panel. The observed values given by ATLAS and CMS are also shown.

fermions is around 0.5 ± 0.3. In the NMSSM, this suppression can be accommodated by the mixing between the singlet and doublet Higgs boson, while keep the couplings to vector weak bosons close to one. In Fig. (3), we also mark out two current global values of $R_{ZZ} \sim (0.7 \pm 0.4)$, $R_{\gamma\gamma} \sim (1.6 \pm 0.4)$ and $R_{ZZ} \sim (1.4 \pm 0.5)$, $R_{\gamma\gamma} \sim (1.8 \pm 0.4)$ given by CMS [2] and ATLAS [1] respectively. For the light stau region which may be helpful to ease this tension, we find the $\delta(g-2)_\mu$ and flavor physics put stringent bounds to the stau mass and $\tan\beta$ in our scanning. The parameter region providing the enhancement by the light chargino/charged Higgs boson to $R_{\gamma\gamma}$ has not been reached since the parameter λ is confined to be less than one in our scanning.

It should be noticed that with the current experimental error bars and statistics, it is too early to conclude that the decay patterns of Higgs boson have confirmed the existence of new physics. As pointed out in Ref. [54], the large uncertainty in the parton distribution function can also affect these results. Future data and reduction in the uncertainty are needed to make sure whether the new physics has been indicated in the Higgs decay modes already.

C. Dark Matter Bounds

In this section, we will discuss the constraints from the DM detections. We assume the LSP and DM candidate is the lightest neutralino. Because the neutralinos have additional singlino component in the NMSSM, the phenomenology of DM is different from that in the MSSM. Especially, the LSP can be pure singlino. In this case, the LSP can be lighter than 100 GeV and can easily escape the constraints from the invisible Z decay measurements due to its almost vanishing coupling to the Z boson. Below we will address the issue whether the singlino in the NMSSM can help to ease the tension between the theories and the experiments.

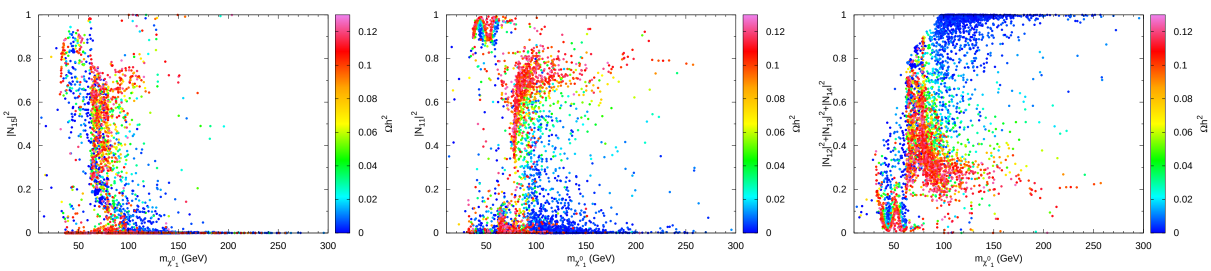

FIG. 4: The Singlino/Bino/(Wino+Higgsino) content of the LSP versus LSP mass. The color scale indicates the LSP relic density.

First, Let's examine the constraints from the dark matter relics density. As we know, the neutralino mass basis $\tilde{\chi}^0_{i=1-5}$ and interaction basis $\psi^0_i = \{\tilde{B}, \tilde{W}, \tilde{H}_d, \tilde{H}_u, \tilde{S}\}$ are related by $\tilde{\chi}^0_i = N_{ij}\psi^0_j$. In the left/middle/right panel of Fig. (4), we show the singlino/bino/Higgsino and wino content $|N_{15}|^2$ $(|N_{12}|^2 + |N_{13}|^2 + |N_{14}|^2)$ of the lightest neutralino, the color scale indicates neutralino thermal relic density $\Omega_\chi h^2$. To obtain the suitable relic density $\Omega_\chi h^2 < 0.1388$, the neutralinos should have enough annihilation cross section $\langle \sigma v \rangle > 3\times 10^{-26}\text{cm}^3\text{s}^{-1}$. In the left panel, we can see the most of lightest neutralinos with significant singlino contents are lighter than 100 GeV. Because the mixing terms between singlino and Higgsinos in the mass matrix are proportional to λ, the LSP as pure singlino means λ is small. In this case, the singlino mass is approximately $2\kappa\mu/\lambda$, the lightest CP-even Higgs and CP-odd Higgs are also singlet-like with small masses. The main DM production mechanism might be

annihilation with s-channel Z resonance or CP-odd/CP-even Higgs resonance [1]. This is the reason why there are many points condensing around the range of $\sim 40-70$ GeV. Moreover, if the λ is not very small, neutralinos could annihilate into light scalar pairs H_1H_1, A_1A_1 or H_1A_1 via the t-channel by the $\tilde{\chi}^0$ exchange or the sufficient large singlet-singlino interaction.

If the lightest neutralino has sufficient Higgsino or wino content, the neutralino annihilation cross section can be large via t-channel chargino exchange to W^+W^-. This is the case for points with $\Omega_\chi h^2 \ll 0.1$ and $m_\chi > 80$ GeV in the right panel of Fig. (4). Because the lightest chargino $\tilde{\chi}_1^+$ can be pure wino or Higgsino. It is also possible to find the parameter points with almost degenerate neutralino $\tilde{\chi}_1^0$ and chargino $\tilde{\chi}_1^+$ which means neutralino can obtain suitable relic density via large co-annihilation $\tilde{\chi}_1^0\tilde{\chi}_1^+$ and $\tilde{\chi}_1^+\tilde{\chi}_1^-$.

Next we consider the constraints from the indirect astrophysics search. If the DM particles annihilate into heavy quarks, charged fermions and gauge bosons at the present time, these annihilation final states can induce significant gamma ray flux which can be detected by air shower cherenkov detectors or satellite detectors. In Fig. (5), we plot parameter points in the $m_{\tilde{\chi}_1^0}$ vs. $\xi^2\langle\sigma v\rangle$ plane. The color scale indicates $\Omega_\chi h^2$. Note that the DM thermal averaged annihilation cross section is rescaled by ξ^2 because the gamma ray flux depends on DM density square and the actual neutralino density may be $\xi\rho_{DM}$. In Fig. (5), the upper-limits derived from Fermi gamma ray observations towards dwarf spheroidal galaxies are also shown [56]. These limits are combined by null results from ten dwarf galaxies, and only a few times above the "natural value" $\langle\sigma v\rangle = 3\times10^{-26}\mathrm{cm}^3\mathrm{s}^{-1}$ for DM with $m_{DM} \sim O(10^2)$ GeV. For parameter points with large wino and Higgsino contents and then large $\langle\sigma v\rangle \gg 3\times10^{-26}\mathrm{cm}^3\mathrm{s}^{-1}$, the thermal neutralino density $\xi\rho_{DM}$ is very small. Thus the reduced annihilation cross section rescaled by ξ^2 can escape the constraints easily. The gamma ray limits become more stringent when DM mass decreases. However, for light neutralino $m_{\tilde{\chi}_1^0} < 70$ GeV with significant singlino content, the annihilation process via s-channel Z or CP-even Higgs exchange is p-wave which is much suppressed at the present universe. Therefore we can see these limits do not exclude many parameter points [2]. The

[1] For the s-channel Z exchange annihilation, small Higgsino content is still needed because $Z\tilde{\chi}_1^0\tilde{\chi}_1^0$ coupling is proportional to $|N_{13}|^2 - |N_{14}|^2$.

[2] The $\langle\sigma v\rangle$ is often estimated at $v \sim 10^{-3}$ which is the typical DM velocity in the present Galactic halo. However, the velocities of DM particles in the dwarf galaxies are about an order of magnitude smaller. When the gamma ray limits from dwarf galaxies are taken into account, this effect needs to be considered for the velocity dependent annihilation cross section [55]. This effect may enhance the cross section signif-

more stringent limits can be derived by Fermi gamma ray observations towards Galactic center, because DM particles are more condensate in this regime. The main problem is how to subtract the complicated astrophysical backgrounds precisely. However, it is possible to improve the constraints to be below the "nature value" for $O(10^2)$ GeV DM in the future.

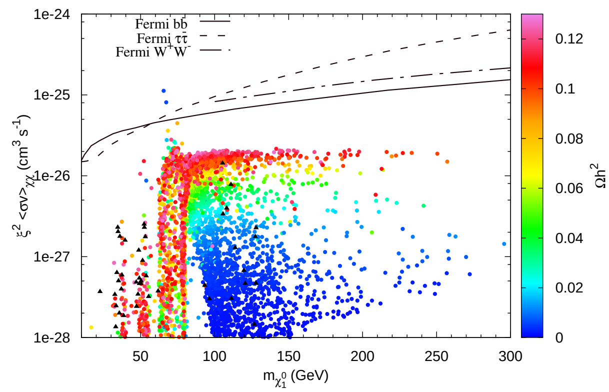

FIG. 5: $\xi^2\sigma v$ versus $m_{\tilde{\chi}_1^0}$. The color scale indicates the neutralino relic density. The black triangles are the LSP with singlino component dominated ($|N_{15}|^2 > 0.8$). The upper limits on three annihilation channels $\chi\chi \to b\bar{b}$, $\tau\bar{\tau}$ and W^+W^- given by Fermi-Lat dwarf galaxies observations are also shown [56].

Then we examine the constraints from the direct searches. We consider both spin-independent and spin-dependent cases. For the spin-independent constraints, we focus on the constraint from the XENON100, which is the most stringent bound for dark matter direct searches. For the spin-dependent constraints, we include bounds from the neutrino flux measurements. In Fig. (6), we plot parameter points in the $m_{\tilde{\chi}_1^0}$ vs. $\xi\sigma_{SI}$ plane. The color scale indicates $\Omega_\chi h^2$. Here $\xi\sigma_{SI}$ is the reduced spin-independent neutralino-nucleon elastic scattering cross section. We also show the most stringent constraints set by XENON100 in 2011 [57] and 2012 [58]. We can see the XENON limits have excluded many parameter points with corrected DM relic density $\Omega_\chi h^2 \sim 0.11$. The spin-independent scattering pro-

icantly when the main annihilation process is s-channel CP-odd Higgs exchange. The large enhancement often requires a very narrow Breit-Wigner resonance with tiny mass splitting parameter $|1-m_A^2/4m_\chi^2| \ll 1$ and decay width $\Gamma_A/m_\chi \ll 1$. This effect would not change our results very much, and is neglected here.

cesses via squark exchanges are strongly suppressed due to the heavy squarks assumed to avoid collider constraints. The main process is the exchange of Higgs through t-channel. The cross section of such process depends on the wino and Higgsino contents of the lightest neutralino and the Higgs masses. Therefore, the neutralinos with masses of $m_\chi > 80$ GeV and intermediate wino and Higgsino contents are strongly disfavored by direct detections, unless the σ_{SI} is reduced by small ξ. Moreover, if the neutralinos have significant singlino contents, and lightest CP-even Higgs is singlet-like, the neutralino-nucleon scattering can be enhanced by additional Higgs-neutralino couplings and small Higgs mass in the propagator. These parameter points might also be easily excluded by XENON limits.

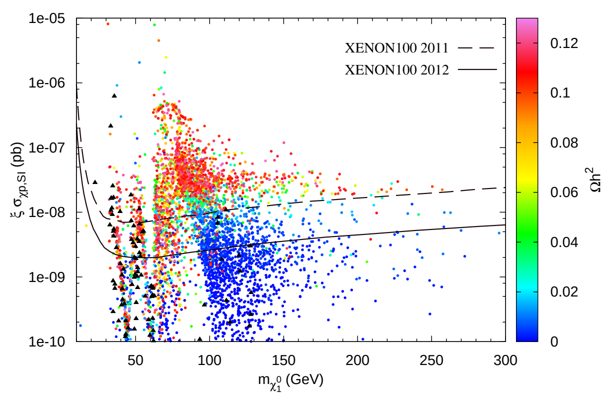

FIG. 6: $\xi\sigma_{SI}$ versus $m_{\tilde{\chi}_1^0}$. The color scale indicates the neutralino relic density. The black triangles are the LSP with singlino component dominated ($|N_{15}|^2 > 0.8$). The upper limits set by XENON100 in 2011 [57] and 2012 [58] are also shown.

For the spin-dependent neutralino-nucleon scattering, the constraints established by direct detections are very weak. The most strong direct constraints given by Coupp [59] and KIMS [60] are of the order of $O(10^{-1})$ pb. More stringent limits can be set by high energy neutrino telescopes. If the DM particles lose their energies by scattering with solar nucleons and are trapped in the center of the sun, they could annihilate into to heavy fermions or gauge bosons and produce detectable high energy neutrino signatures. The signature flux can be determined by DM-nucleon spin-dependent scattering rate. Moreover, it also depends on the fractions of certain DM annihilation channels $f_i = \sigma(\chi\chi \to X_i X_i)/\sigma_{\chi\chi}$ which

could produce neutrinos. In the left (right) panel of Fig. 7, we present the parameter points in the $m_{\tilde{\chi}_1^0}$ vs. $\xi\sigma_{SD}$ ($m_{\tilde{\chi}_1^0}$ vs. $\xi\sigma_{SD}f_{VV}$) plane. The limits given by Coupp [59], Superk [61] and IceCube [62] are also shown. Note that the neutrino energy spectra from different DM annihilation channels are different, the limits from neutrino telescopes are derived from experimental results for different channels. Because the neutrino energy spectra from $b\bar{b}$ ($q\bar{q}$, $\tau\bar{\tau}$) are much softer than those from W^+W^- (ZZ, $t\bar{t}$), the limits from W^+W^- channel are more stringent. From the left panel of Fig. (7), we can see recent direct detections and neutrino signatures from soft channels do not constrain models very much. However, if the neutralinos have intermediate Higgsino contents, the spin-dependent cross section might be large due to $Z\tilde{\chi}_1^0\tilde{\chi}_1^0$ coupling which is proportional to $|N_{13}|^2 - |N_{14}|^2$. In this case, some parameter points with $\xi\sigma_{SD} > O(10^{-4})$pb and $f_{VV} \sim 1$ have been excluded. The expected limit which can be set by IceCube 86 strings are also shown. We can see the IceCube has the capability to exclude most of the parameter points which predict neutralinos with significant Higgsino contents and correct DM relic density $\Omega_\chi h^2 \sim 0.11$.

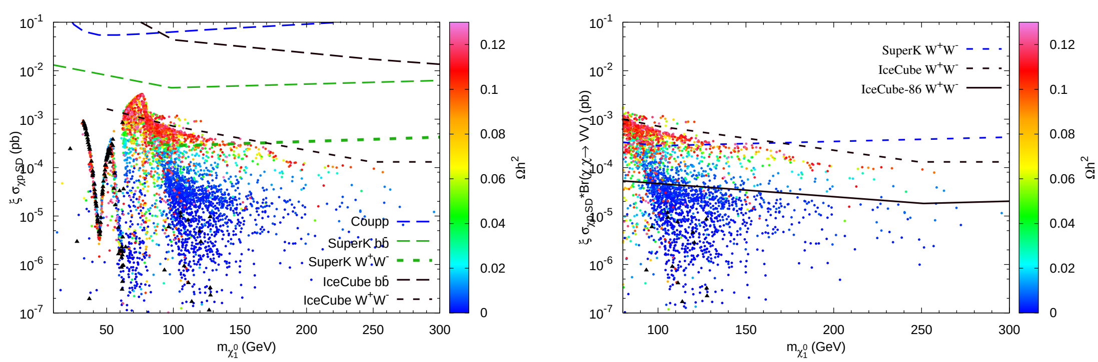

FIG. 7: Left: $\xi\sigma_{SD}$ versus $m_{\tilde{\chi}_1^0}$. Right: $\xi\sigma_{SD}f(\tilde{\chi}_1^0\tilde{\chi}_1^0 \to VV)$ versus $m_{\tilde{\chi}_1^0}$. The color scale indicates the neutralino relic density. The black triangles are the LSP with singlino component dominated ($|N_{15}|^2 > 0.8$).. The limits given by Coupp [59], Superk [61] and IceCube [62] are also shown.

To examine the impact of singlino to the dark matter searches, in Fig. (5-7), we have marked out those allowed points with dominant singlino constituent by the black triangles. It is observed that when the LSP is singlino dominant, it can escape the constraint from Fermion LAT easily, as demonstrated in Fig. (5). While the bounds from XENON100 2011

and 2012 are really impressive and can exclude a certain fraction of those allowed points even the LSP is singlino dominant. For the neutrino bounds, since many LSP with singlino dominant are lighter than W boson, they can be still consistent with data due to weak constraints from $b\bar{b}$ channel. For the LSP heavier than W boson, the annihilation cross section of $\tilde{\chi}^0\tilde{\chi}^0 \to W^+W^-$ is always small enough and can be safe. From the analysis shown above, we can see that the singlino/bino in the NMSSM can help to ease the tension between theories and experiments, while the wino and Higgsino like dark matter candidates are more constrained.

III. LHC SUSY SEARCH BOUNDS

A. The production and decay of light stop/sbottom at LHC

In this section we study the SUSY search bounds on the light stop/sbottom pair signatures from LHC. For our purpose below we make two additional requirements for the parameter points past all constraints in Sec II. First, we require the stop mass should be lighter than 500 GeV in order to have a large enough production rate. Since we have assumed $m_{U_3} = m_{D_3}$, so the lightest sbottom is light in our analysis. Then the largest color sparticle signatures are the stop pair and sbottom pair productions. Second, to accommodate the SM-like Higgs in the NMSSM, we require $R_{VV} + R_{\gamma\gamma} > 1.8$ in the parameter space. Implicitly, this condition also means that the branching ratios of the exotic Higgs decay modes should not be very large. Consequently, it also suggests that the lightest neutralino, CP-odd and CP-even Higgs can not be very light. This feature will also affect the decays of other sparticles. After taking into account these two extra requirements, we choose 647 parameter points that survived all our criteria for our simulations. Below we study the constraints from direct SUSY searches at LHC to these points.

In the left panel of Fig .(8), we show the cross section of stop pair production $\sigma_{\tilde{t}\tilde{t}}$ at the LHC with $\sqrt{s} = 7$ TeV. Here we use the package Prospino2 [63] to calculate $\sigma_{\tilde{t}\tilde{t}}$ including the next leading order corrections. Because the main production channel of stop pair at the LHC is $gg \to \tilde{t}\tilde{t}$, we can see $\sigma_{\tilde{t}\tilde{t}}$ is uniquely determined by stop mass. For the stop with mass of $m_{\tilde{t}} \leq 500$ GeV, the $\sigma_{\tilde{t}\tilde{t}}$ is larger than 45 fb, and there would be more than ~ 200 stop pair events at the LHC with 5 fb^{-1} of data.

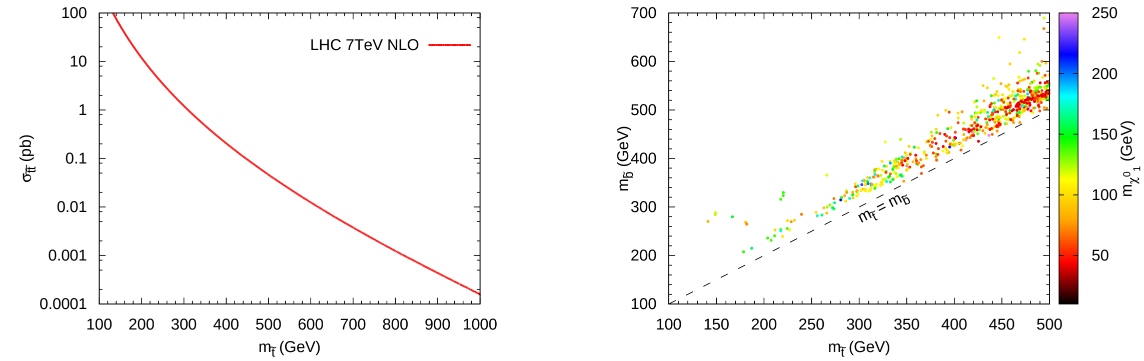

FIG. 8: Left: the NLO cross section of stop pair production as a function of stop mass. Right: sbottom mass versus stop mass, where the color scale indicates neutralino mass.

The masses of stop and sbottom are shown in the right panel of Fig. (8) where the color scale indicates the lightest neutralino mass. We can see the mass splitting between stops and sbottoms are small due to our assumption $m_{U_3} = m_{D_3}$ and the lighter stop and sbottom quarks are either dominantly left-handed or right-handed. It is supposed that this parameter configuration can pass the electroweak precision tests easily [13, 64].

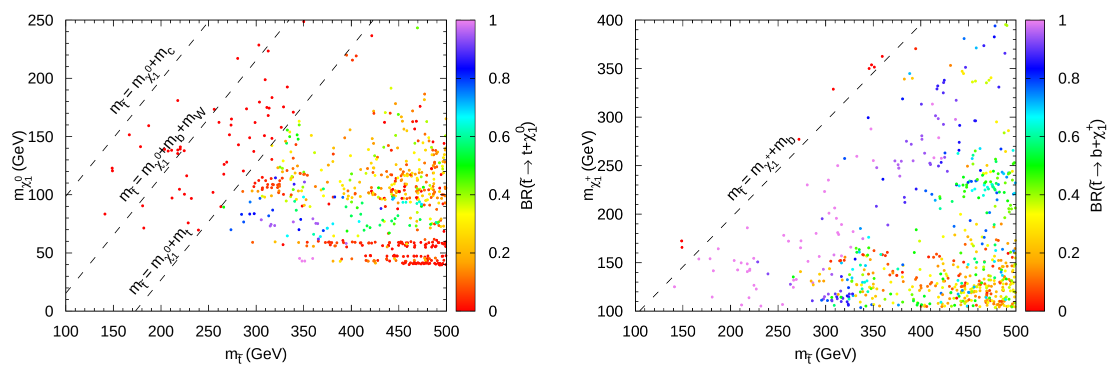

FIG. 9: The lightest neutralino/chargino mass versus stop mass in the left/right panel. The color scale indicates the branching ratio of stop $\mathrm{BR}(\tilde{t} \to t\tilde{\chi}_1^0)/\mathrm{BR}(\tilde{t} \to b\tilde{\chi}_1^+)$ in the left/right panel.

The stop decay pattern is dominantly determined by the mass splitting between the stop

and light neutralinos/charginos. If the stop is much heavier than the lightest neutralino and chargino, the main decay channels are two body decays $\tilde{t} \to t\tilde{\chi}_1^0$ and $\tilde{t} \to b\tilde{\chi}_1^+$. In Fig. (9), we show the relations between the sparticle mass spectra and the branching ratios of $\tilde{t} \to t\tilde{\chi}_1^0$ and $\tilde{t} \to b\tilde{\chi}_1^+$. We can see the decay modes depend on the neutralino and chargino mass spectra. The processes of stop decay into $t\tilde{\chi}_2^0$, $t\tilde{\chi}_3^0$ and $b\tilde{\chi}_2^+$ might be also significant for heavy stop (as demonstrated in first two bench mark points given in Table. (VII)). In this case, even the LSP is very light < 100GeV, decay mode $\tilde{t} \to t\tilde{\chi}_1^0$ may also be suppressed. These processes have longer decay chains than $\tilde{t} \to t\tilde{\chi}_1^0$, and produce softer final states. When the mass splitting is too small to forbid above two body decays, the three body decay channels $\tilde{t} \to bW\tilde{\chi}_1^0$ and $\tilde{t} \to b\nu\tilde{l}/bl\tilde{\nu}$ become important. If these processes are also kinematic forbidden, the loop induced two body FCNC decay $\tilde{t} \to c\tilde{\chi}_1^0$ would be dominant. Moreover, the four final state decay modes $\tilde{t} \to bj_1j_2\tilde{\chi}_1^0$ and $\tilde{t} \to b\ell\nu_\ell\tilde{\chi}_1^0$ are also possible if the W boson in the three body decay mode is not on-shell.

The main two-decay modes of sbottom include $\tilde{b}_1 \to b\tilde{\chi}_i^0$ and $\tilde{b}_1 \to t\tilde{\chi}_i^-$. The three-body decay modes include $\tilde{b}_1 \to t^*\tilde{\chi}_i^- \to bW^+\tilde{\chi}_i^-$. The decay chain of sbottom can be quite long and all the final state from its decay can be soft as demonstrated in the third bench mark points in Table. (VII).

B. constraints on stop/sbottom pair signatures

The general SUSY search bounds for squarks and gluino have been provided by ATLAS and CMS, corresponding to an integrated luminosity of $2 \sim 5$ fb^{-1}. In this subsection, we investigate the constraints on light stop pair and sbottom pair productions based on these results. In our studies, parton-level events $pp \to \tilde{t}\tilde{t}$ and $pp \to \tilde{t}\tilde{t} + jets$ are generated by MADGRAPH5 [65]. PYTHIA [66] is used to perform the parton shower, decay, final state radiation, and hadronization processes. The detector effects are simulated by PGS4 [67]. To avoid the double-counting issue, we adopt the MLM matching scheme and choose $Q_{cut} = 80$ GeV in our simulation. Jet candidates are reconstructed by using the anti-kt jet algorithm (which is infrared and collinear safe) with a distance parameter of 0.4/0.5 for the ATLAS/CMS searches [3].

[3] The basic selected conditions for jets and leptons are slightly changed in different searches. In general, these conditions are $p_t > 20-40$ GeV, $|\eta| < 2.5-3$ for jets, $p_t > 10-25$ GeV, $|\eta| < 2.0-2.5$ for electrons

Currently, most of experimental groups from both CMS and ATLAS collaborations work in the simplified model. The signals are assumed to be $pp \to \tilde{b}_1\tilde{b}_1^* \to b\bar{b}\chi_1^0\chi_1^0$ or $pp \to \tilde{t}_1\tilde{t}_1^* \to t\bar{t}\chi_1^0\chi_1^0$. It is interesting to examine what might happen in a concrete model like the NMSSM and how new decay modes can be affected by these direct searches. We will consider two categories of constraints from the direct search: 1) the searches for the final states without b-jets; 2) the searches for the final states with b-jets.

1. Constraints for Final states without b-jets

If the dominated decay modes of squarks and gluino are $\tilde{q} \to q\tilde{\chi}_1^0$ and $\tilde{g} \to q\bar{q}\tilde{\chi}_1^0$, the main features of events are energetic jets and large MET. This signature channel can set the most stringent constraints on CMSSM and simplified model without light stop/sbottom. For the light squarks of the third generation, such signatures would be suppressed due to smaller production cross section and different decay modes. Because such analysis requires very hard jets and large MET, the events of stop pair with many soft jets can escape the constraints easily. Below we investigate how the m_{eff} and $\not{E}$ cuts as well as the associated mono-jet searches can affect our selected points.

and muons. Moreover, the electron candidates in the barrel-endcap transition region with $1.44 < \eta < 1.57$ are rejected. Here we used the basic selections as adopted by ATLAS and CMS according to different researches, and do not list them in the following discussions.

Requirements	A	A'	B	C	D	E
$\not{E}_T$ [GeV] $>$	160					
$N_{Jet}(p_T > 130$ GeV$) \geq$	1					
$N_{Jet}(p_T > 60$ GeV$) \geq$	2	2	3	4	4	4
$N_{Jet}(p_T > 40$ GeV$) \geq$	-	-	-	-	5	6
$\Delta\phi(\vec{j}_i, \vec{\not{E}}_T)_{min} >$	0.4 (i=1,2,(3))			0.4 (i=1,2,3), 0.2 ($p_T^j > 40$ GeV)		
$\not{E}_T/m_{eff}(N_{Jet}) >$	0.3 (2j)	0.4 (2j)	0.25 (3j)	0.25 (4j)	0.2 (5j)	0.15 (6j)
m_{eff}(incl.) [GeV] $>$	1900/1400/-	-/1200/-	1900/-/-	1500/1200/900	1500/-/-	1400/1200/900
N_{lim}^{obs}	2.9/25/-	-/29/-	3.1/-/-	16/18/58	10/-/-	12/12/84

TABLE I: Summary of cuts and observed 95% CL upper limits on the excess event number, following the ATLAS jets+MET analysis for 4.7 fb^{-1}[23].

The first constraint is from the jets plus missing energy searches. We list the cut conditions adopted by ATLAS collaboration in Table. (I) [23]. This analysis is based on 4.7 fb^{-1} of data, and all the events with isolated electrons or muons are rejected. The azimuthal angle $\Delta\phi(\vec{j}_i, \vec{\not{E}}_T)$ is defined as the azimuthal angle separation between the $\not{E}_T$ and the jets. The effective mass is defined as

$$m_{eff} = \not{E}_T + \sum_{i=1}^{N_j} p_T^j + \sum_{i=1}^{N_l} p_T^l. \tag{11}$$

It is obvious to see the effective mass characterizes the mass scale of SUSY particles directly produced by pp collisions. Large $m_{eff} \sim$ 1TeV is helpful to reduce the SM backgrounds, such as $W + jets$, $Z + jets$, $t\bar{t}$ and single top, but it also suppresses light stop/sbottom pair events with soft jets severely.

For each signal region, three m_{eff} cut conditions (denoted by 'tight/medium/loose') are taken into account. In Table. (I), the 95% C.L. observed upper limits N_{lim} on number of new physics events given by experimental collaboration are also listed [23]. For comparison, we show the ratio of predicted event number N to upper limit N_{lim} in Fig. (10) where the color scale denotes the LSP mass [4]. Here we have summed the signature of stop pair and sbottom pair together. If the m_{eff} cut is chosen to be too large, most of the signals

[4] It should be noticed that the bounds shown in our analysis have not included theoretical and experimental

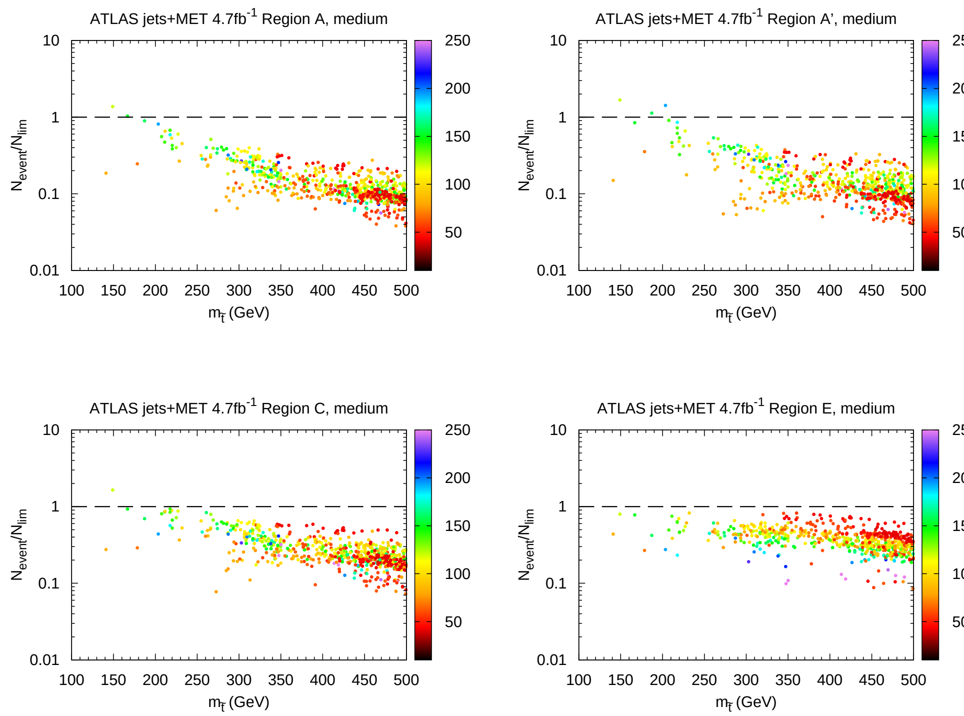

FIG. 10: The ratio of $\tilde{t}\tilde{t}^{*}+\tilde{b}\tilde{b}^{*}$ event number and observed 95% CL upper limit versus stop mass in the signal regions A, A', D, E. The color scale indicates neutralino mass.

would be rejected. Otherwise, there are too many background events which leads to a much weaker the upper-limits for new physics. Better constraints can be demonstrated by the four medium channels A, A', C and E in Fig. (10).

We have also checked the results for all the channels, and find jets+MET channel can set marginal constraints on the most of parameter points when the stop mass is below ~ 200 GeV and the main decay mode is $\tilde{t} \to c\tilde{\chi}_1^0$. The large cross section of stop pair production $\sim$ O(10) pb can induce event excess, as indicated in A and A' region in Fig. (10). Interestingly, it is noticed that some parameter points with light LSP and stop can not be excluded by this search. These parameter points also predict light charginos, sleptons or second neutralino, therefore the decay chain can be long and the final states contain less hard jets, which can hide into the background events, as shown in all regions of Fig. (10).

errors. Although our simulated results are close to those experiment ones, it should be remembered that when these uncertainties are taken into account, the lines should become to be bands.

We can see there are quite a fraction of points in A and A' situated below $N/N_{lim} = 0.1$, while all those points are above $N/N_{lim} = 0.1$ in C and E. For the heavier stop with dominated decay mode $\tilde{t} \to t\tilde{\chi}_1^0$, the channels requiring high jet multiplicity should be more efficient. For instance, we can read out the values of N/N_{lim} is only close to 1.0 for red parameter points with $m_{\tilde{t}} > 350$ GeV and $m_{\tilde{\chi}_1^0} < 100$ GeV in the region E-medium presented in Fig. (10).

We also check the constraints from ATLAS jets+MET research based on 1 fb^{-1} of data [68]. In this analysis, the m_{eff} cut is required to be O(100) GeV. Considering the huge SM backgrounds prevent from setting a better constraint to stop/sbottom mass, we find the N/N_{lim} is much lower, e.g. <O(10^{-1}).

$N_{Jet}(p_T > 100)$	$N_{Jet}(p_T > 30)$	$\Delta\phi(j_1, j_2)$	$\not{E}_T$	N_{lim}^{obs}
≥ 1	≤ 2	≤ 2.5	$>$ 250/ 300/ 350/ 400	600/ 368/ 158 /95

TABLE II: Summary of cuts and observed 95% CL upper limits on the excess event number, following the CMS mono-jet+MET analysis for 4.98 fb^{-1} [71].

The second constraint which will be considered here is from the associated mono-jet production. As is well-known, when the dark matter particles are directly produced by pp collisions, one possible search channel is the mono-jet + MET [69]. The mono-jet is produced by the initial state radiation and can be energetic. If stop is nearly degenerate with the LSP, the soft jets from stop decay might not be reconstructed by the detectors. In this case, the stop production $\tilde{t}\tilde{t}j$ can be constrained by mono-jet + MET research [27, 28, 70]. The cut conditions and upper-limits given by CMS are summarized in Table. (II) [71]. This analysis is based on 4.98 fb^{-1} of data, and all the events with isolated electrons or muons are rejected.

In Fig. (11), we show the ratio N/N_{lim} with both $\not{E} > 350$ GeV and $\not{E} > 400$ GeV cases. For these large $\not{E}_T$ cut conditions, the jet from the initial state radiation is required to be very energetic $p_j^T \sim \not{E}_T$. It is obvious to see only light stop with $m_{\tilde{t}} < 200$ GeV and large production cross section can have large event rate, as demonstrated in Fig. (11). For heavier stops with $\tilde{t} \to t\tilde{\chi}_1^0$, cut condition on the third jet will suppress the events with high jet multiplicities and leads to a weaker constraint. For the sbottom which is not degenerate with LSP, the dominated decay mode can be $\tilde{b} \to b\tilde{\chi}_1^0$. Therefore, the cuts on transverse momentum of jets can be satisfied easily. But the sbottom pair can not induce large $\not{E}_T$

signal as required in this analysis which also leads to a weaker constraint.

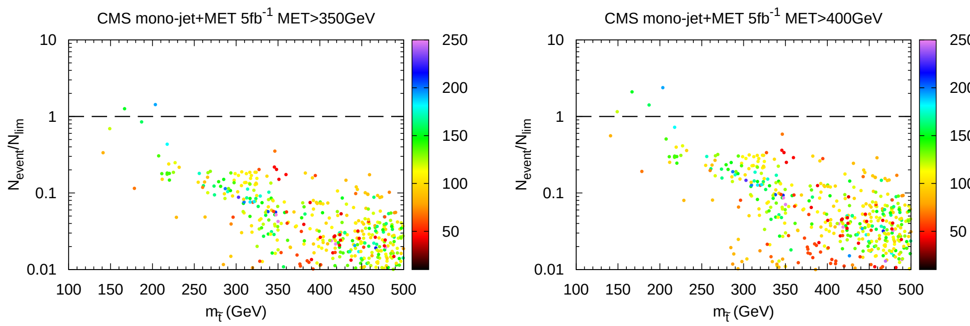

FIG. 11: The ratio of $\tilde{t}\tilde{t}^{*}$+$\tilde{b}\tilde{b}^{*}$ event number and observed 95% CL upper limit versus stop mass in the signal regions for $\not{E}_T > 350$ GeV and $\not{E}_T > 400$ GeV. The color scale indicates neutralino mass.

2. Constraints for Final states with b-jets

In this subsection, we explore the impact of b-jets+MET searches on stop/sbottom pair production signatures. The identification of b-jet is helpful to reduce the huge QCD backgrounds. In this case, the dominated SM backgrounds are top pair production and associated production of W/Z with heavy flavor jets. The di-bosons production WW, ZZ and WZ are sub-dominated due to smaller electro-weak cross section.

As discussed in Ref. [6], the "naturalness" of SM-like Higgs mass suggests a light stop $\leq$ 700 GeV and a not very heavy gluino $\sim$ 1 TeV in the SUSY model. In this case, the gluino pair production has a moderate cross section, and the cascade decay productions would contain many top and bottom quarks. For example, the typical SUSY search channels are $\tilde{g}\tilde{g} \to t\bar{t}\tilde{t}\tilde{t}^{*} \to tt\bar{t}\bar{t} + MET$ or $\tilde{g}\tilde{g} \to b\bar{b}\tilde{b}\tilde{b}^{*} \to bb\bar{b}\bar{b} + MET$. The multi-b jets in the final states are very powerful to suppress the SM backgrounds. Therefore, the LHC has strong capability to test or exclude such scenario.

In this work, we have assume the gluino is very heavy $>$ 1.5 TeV. Therefore the main production signatures are $pp \to \tilde{t}_1\tilde{t}_1^{*}$ and $pp \to \tilde{b}_1\tilde{b}_1^{*}$. For the light sbottom pair production, the b-jets+MET search can constrain the channel $\tilde{b}\tilde{b} \to b\bar{b} + MET$ if the $\Delta m_{\tilde{b}} = m_{\tilde{b}} - m_{\tilde{\chi}_1^0}$ is large enough (say larger than 50 GeV). For the stop pair production, if the dominated

stop decay mode is $\tilde{t} \to bW\tilde{\chi}$ or $\tilde{t} \to t\tilde{\chi} \to bW\tilde{\chi}$, the b-jets in final states are less energetic. To pass the p_T cut on the leading b-jet, the $\Delta m_{\tilde{t}} = m_{\tilde{t}} - m_{\tilde{\chi}_1^0}$ is required to be large, and the detectable capability is lower than that of sbottom pair. Here we point out that if the chargino is light and light stop has large left-handed component, the $\tilde{t} \to b\tilde{\chi}_1^+$ can become significant. Especially, if the chargino mass is nearly degenerate with LSP which can be used to obtain required DM relic density through co-annihilation mechanism, the kinematics of $\tilde{t} \to b\tilde{\chi}_1^+$ is very similar to the $\tilde{b} \to b\tilde{\chi}_1^0$. In this case, the b-jets+MET search is also useful to test or exclude stop pair signatures. This feature is also addressed in the first bench mark point in Ref. [72].

$p_T^{bjet_1}$	$p_T^{bjet_2}$	$p_T^{j_3}$	$\Delta\phi(\vec{j}_i, \vec{\not{E}}_T) >$	$\not{E}_T >$	$\not{E}_T/m_{eff}^{N_j=2} >$	$m_{CT} >$	N_{lim}^{obs}
> 130	> 50	< 50	0.4(0.2) (i=1,2,(3))	130	0.25	100/150/200	27.5/19.7/11.5

TABLE III: Summary of cuts and observed 95% CL upper limits on the excess event number, following the ATLAS 2b-jets+MET analysis for 2.05 fb^{-1}[73].

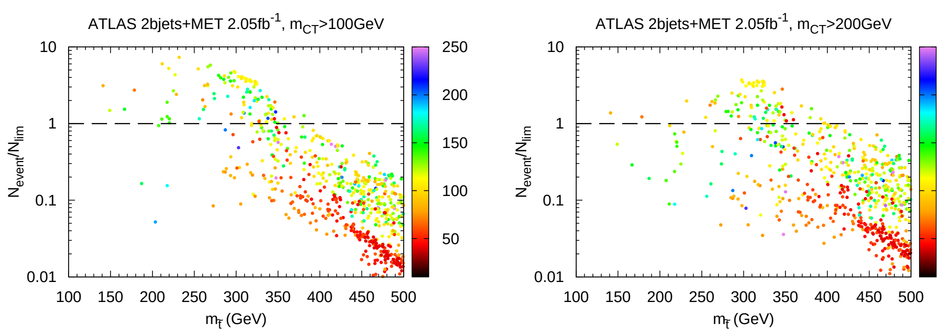

FIG. 12: The ratio of $\tilde{t}\tilde{t}^*$+$\tilde{b}\tilde{b}^*$ event number and observed 95% CL upper limit versus stop mass in the signal regions for $m_{CT} > 100$ GeV and $m_{CT} > 200$ GeV. The color scale indicates neutralino mass.

First, we consider the ATLAS 2b-jets+MET search based on 2.05 fb^{-1} of data [73]. This search is optimized for sbottom pair production with sbottom branching ratio of $BR(\tilde{b} \to b\tilde{\chi}_1^0) = 100\%$. The corresponding cut conditions and limits are summarized in Table. (III). In this analysis, the number of jets with $p_t > 50$ GeV is required to be exactly two. No m_{eff}

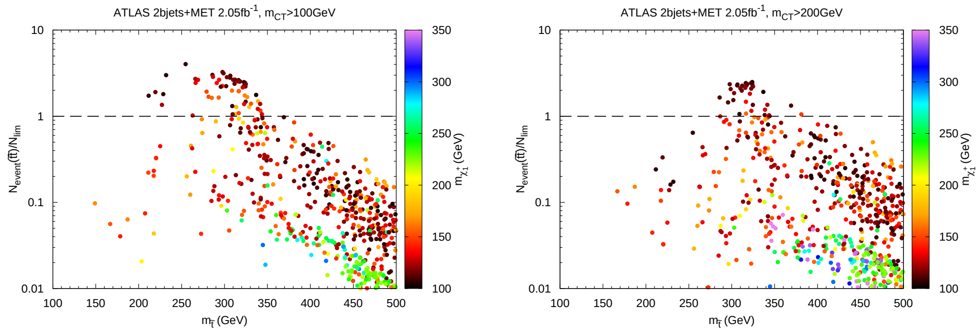

FIG. 13: The ratio of $\tilde{t}\tilde{t}^*$ event number and observed 95% CL upper limit versus stop mass in the signal regions for $m_{CT} > 100$ GeV and $m_{CT} > 200$ GeV. The color scale indicates chargino mass.

cut is imposed because sbottom should be light to provide large production cross section. A boost-corrected con-transverse mass m_{CT} is introduced [74]

$$m_{CT} = \sqrt{(E_T^{j_1} + E_T^{j_2})^2 - (\vec{p}_T^{j_1} - \vec{p}_T^{j_1})^2}, \tag{12}$$

where m_{CT} is invariant under contra-linear equal magnitude boosts. It can be expected that the distribution of m_{CT} display an endpoint at $(m_{\tilde{b}}^2 - m_{\tilde{\chi}_1^0}^2)/m_{\tilde{b}}$ when two b-jets are co-linear. In Fig. (12), the ratios N/N_{lim} are shown . We find this search can exclude many selected parameter points, especially when the mass splitting $\Delta m_{\tilde{b}} = m_{\tilde{t}} - m_{\tilde{\chi}_1^0}$ is large enough with $m_{\tilde{t}_1}$ in the range from 250 GeV to 350 GeV. When comparing the left and right panel of Fig. (12), it is easy to read out the fact that the smaller m_{CT} is more sensitive to smaller stop/sbottom mass region. It might be interesting to notice that the maximum excluded $m_{\tilde{t}_1}$ can reach to 380 GeV by this observable.

Moreover, we show the ratios N/N_{lim} only for stop pair production in Fig. (13) where the color scale indicates the mass of chargino $\tilde{\chi}_1^+$. It is noticed that even if sbottom is very heavy, the 2-bjets search can be useful to put constraints on stop pair production. This can occur for the points with significant decay mode $BR(\tilde{t} \to b\tilde{\chi}_1^+)$ with very small $m_{\tilde{\chi}_1^+} - m_{\tilde{\chi}_1^0}$, as we have mentioned before.

It should be noted that the $BR(\tilde{t} \to b\tilde{\chi}_1^+)$ can not simply be determined by $m_{\tilde{\chi}_1^+}$. When the mass of LSP $m_{\tilde{\chi}_1^0}$ is much smaller than that of lighter chargino $m_{\tilde{\chi}_1^+}$, the decay mode $\tilde{t} \to t\tilde{\chi}_1^0$ is still significant. Furthermore, if the kinematics is allowed, other decay modes $\tilde{t} \to t\tilde{\chi}_2^0$ and $\tilde{t} \to b\tilde{\chi}_2^+$ are open and can reduce the decay mode $BR(\tilde{t} \to b\tilde{\chi}_1^+)$. For both

cases, the constraints from this search become weaker or even invalid.

Requirements	N_l	$N_{bjet} \geq$	$p_T^{j_1}$	$p_T^{j_{2,3}}$	$p_T^{j_4}$	$m_T >$	$\not{E}_T >$	$\not{E}_T/m_{eff} >$	$\Delta\phi >$	$m_{eff} >$	N_{lim}^{obs}
SR0-A1/B1/C1	0	1	> 130	> 50	-	-	130	0.25	0.4	500/700/900	580/133/31.6
SR0-A2/B2/C2	0	2	> 130	> 50	-	-	130	0.25	0.4	500/700/900	124/29.6/8.9
SR1-D	1	1	> 60	> 50	>50	100	80	-	-	700	45.5
SR1-E	1	1	> 60	> 50	>50	100	200	-	-	700	17.5

TABLE IV: Summary of cuts and observed 95% CL upper limits on the excess event number, following the ATLAS b-jets+MET analysis for 2.05 fb^{-1} [75].

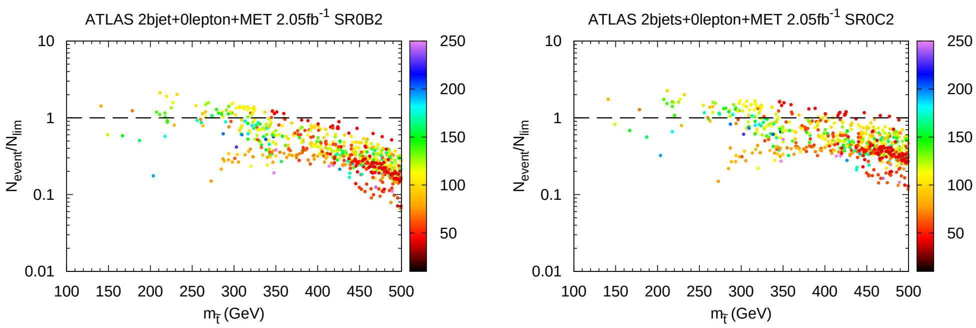

FIG. 14: The ratio of $\tilde{t}\tilde{t}^{*}+\tilde{b}\tilde{b}^{*}$ event number and observed 95% CL upper limit versus stop mass in the signal regions SR0-B2 and SR0-C2. The color scale indicates neutralino mass.

Next, we consider the ATLAS b-jets+MET search based on 2.05 fb^{-1} of data [75]. In this analysis, the number of b-jets is required to be at least one or two. Moreover, two signal regions allow one lepton in the final states. This search can be supposed to constrain the the signal $pp \to \tilde{t}_1\tilde{t}_1^{*}$. The corresponding cut conditions and limits are summarized in Table. (IV). The ratios N/N_{lim} from two most stringent channels SR0B2 and SR0C2 are shown in Fig. (14). We can see even these channels require a large m_{eff} cut as $m_{eff} > 700-900$ GeV, they can still exclude many parameter points. It is remarkable that the channel SR0B2 (SR0C2) can exclude signals with maximum $m_{\tilde{t}_1}$ up to 380 GeV(480 GeV). The constraints from 1b-jet+MET signal regions are weaker than 2b-jets+MET due to the large backgrounds. The lepton + b-jets + MET in the same analysis also can not achieve better

constraints and are omitted here.

Requirements	$p_T^{j_{1,2,3}}$	$\Delta\phi_{norm}$	$N_{bjet} \geq$	H_T	$\not{E}_T$
1BL	>50	4.0	1	400	250
1BT	>50	4.0	1	500	500
2BL	>50	4.0	2	400	250
2BT	>50	4.0	2	600	300

TABLE V: Summary of cut conditions, following the CMS b-$jets + MET$ analysis for 4.98 fb^{-1}. The capital letter "L" and "T" means "loose" and "tight" respectively.

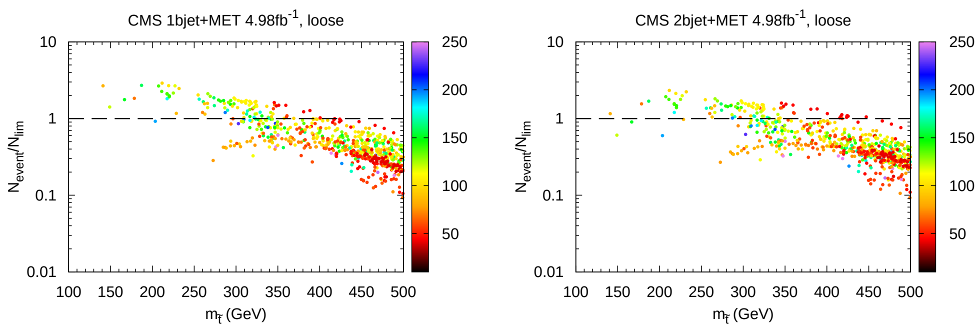

FIG. 15: The ratio of $\tilde{t}\tilde{t}^* + \tilde{b}\tilde{b}^*$ event number and observed 95% CL upper limit versus stop mass in the signal regions 1BL and 2BL. The color scale indicates neutralino mass.

Then we consider CMS b-jets+MET search based on 4.98 fb^{-1} of data [76]. The corresponding cut conditions are summarized in Table. (V). In this analysis, H_T defined as scalar sum of momenta of all the energetic jets are used to set cut conditions. $\Delta\phi_{norm}$ is normalized azimuthal separation between $\not{E}$ direction and jets. The collaboration has not yet provided limits on the number of new physics explicitly. Here we use the formula given in Ref. [69] to roughly estimate the upper-limits,

$$\chi^2 = \frac{[N_{obs} - N_{SM} - N_{BSM}]^2}{N_{BSM} + N_{SM} + \sigma_{SM}^2} \tag{13}$$

where N_{obs} is the number of observed events, N_{SM} and σ_{SM} are the predicted background number and the uncertainty due to statistic and systematic reasons respectively. Requiring

$\chi^2 < 3.84$, we can get the upper-limits on four channels as 124, 14.7, 58 and 41 respectively. Because this analysis dose not require very hard leading jet, the numbers of events passing all the cuts conditions are larger than last analysis. The ratios N/N_{lim} are given in Fig. 15. Because the "tight" cut conditions require very large $\not{E}$, the signals are significant reduced in these signal regions. Here we only show the constraints from "loose" searches.

The bounds obtained from inclusive and exclusive 2-bjets+MET searches can be compared from Fig. (12), Fig. (16) and Fig. (15). Roughly speaking, the bounds from inclusive 2-bjets+MET searches seem to be more stringent, as demonstrated by the fact the selected points are squeezed in a smaller range of N/N_{lim} between 0.1 and 1 and the maximum excluded $m_{\tilde{t}_1}$ can reach to ~ 400 GeV.

Requirements	$p_T^{j_1} >$	$p_T^{j_2} >$	$p_T^{j_3} >$	$p_T^{j_4} >$	$\phi(\vec{j}_{1,2}, \vec{\not{E}}_T) >$	m_{jjj}	$\not{E}_T >$	$\not{E}_T/\sqrt{H_T} >$	$m_T >$	N_{lim}
A/B/C	80	60	40	25	0.8	[130, 205]	150	7/9/11	120	15.1/10.1/10.8
D	80	60	40	25	0.8	[130, 205]	225	11	130	8.4
E	80	60	40	25	0.8	[130, 205]	275	11	140	8.2

TABLE VI: Summary of cuts and observed 95% CL upper limits on the excess event number, following the ATLAS "heavy top" 1lepton+b-jets+MET analysis for 4.7 fb^{-1} [76].

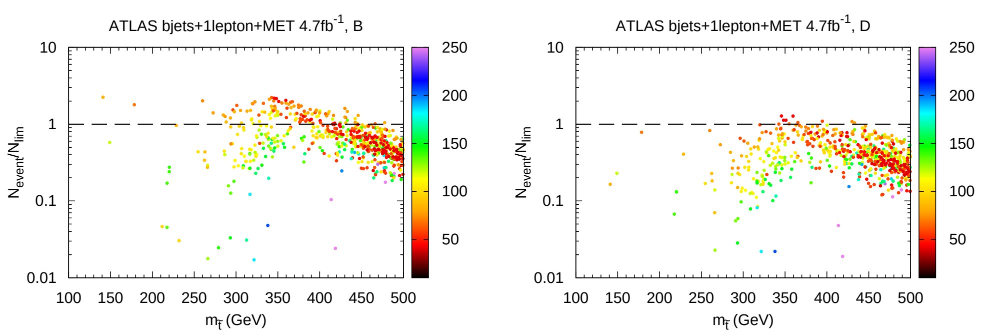

FIG. 16: The ratio of $\tilde{t}\tilde{t}^* + \tilde{b}\tilde{b}^*$ event number and observed 95% CL upper limit versus stop mass in the signal regions B and D. The color scale indicates neutralino mass.

Since the semileptonic mode of $pp \to \tilde{t}_1\tilde{t}_1^* \to t\bar{t}\tilde{\chi}_1^0\tilde{\chi}_1^0$ can have a large branching fraction and enjoys a smaller SM background, so it is expected the search for this mode should

be stringent. Then we consider the constraints from ATLAS 1lepton+b-jets+MET searches based on 4.7 fb^{-1} of data [77] [5]. The corresponding cut conditions and limits are summarized in Table. (VI). It requires that the number of isolated lepton is exactly one. Obviously, this analysis is optimized for searching stop pair production with decay mode $\tilde{t} \to t\tilde{\chi}_1^0$. One top from stop decay is required to decay hadronically and the other semileptonically. m_T is the transverse mass defined as

$$m_T = \sqrt{2p_T^l \not{E} (1 - \cos \Delta\phi(l, \vec{\not{E}}_T))}. \tag{14}$$

m_T denotes the mass scale of mother particles which decay into charged leptons, and m_T cut can be used to reduce $W + jets$ backgrounds. To suppress the backgrounds from dileptonically decaying top pair, a specific cut on three-jet invariant mass m_{jjj} is required. Two jets with $m_{jj} > 60$ GeV and smallest ΔR are assumed to be originated from a hadronically decaying W boson, and a third jet which is closest to the reconstructed W boson is selected. These three jets may be the decay products of a hadronically decaying top, and the invariant mass m_{jjj} is required to be around top mass 130 GeV$< m_{jjj} <$ 205 GeV.

The ratio N/N_{lim} is shown in Fig. (16). It is obvious that this channel is sensitive to the mass range of stop from 270 GeV to 400 GeV, when the main decay mode of stop can be $\tilde{t} \to t\tilde{\chi}_1^0$. On the other hand, for the parameter points with heavy stop $>$ 400 GeV and light LSP $<$ 150 GeV in our scan, the main decay mode of stop $\tilde{t} \to t\tilde{\chi}_2^0$, $\tilde{t} \to t\tilde{\chi}_3^0$ or $\tilde{t} \to b\tilde{\chi}_2^+$ are open. In this case, although the mass difference between stop and LSP is large, the limits becomes weaker due to the absence of energetic top quarks in the final states. From Fig. (16) we can also see the constraints from signal region B are more strong than region E due to the smaller $\not{E}$ cut condition.

In Fig. (17), we summarize the most stringent bounds from direct SUSY searches for both stop and sbottom pair productions. It is observed that for the stop pair production, the current LHC collaborations can exclude stop(sbottom) up to 400 GeV or so when only the exclusive signals are considered. While when the inclusive signals are considered, the direct searches can exclude the mass of stop up to 500 GeV, as shown by the bottom right plot.

[5] The ATLAS analysis of 0 lepton+b-jets+MET in Ref. [78] is also optimized for stop pair production with decay mode $\tilde{t} \to t\tilde{\chi}_1^0$, while tops are assumed to decay hadronically. The constraints from this channel are weaker than the semileptonic channel over most of the parameter space.

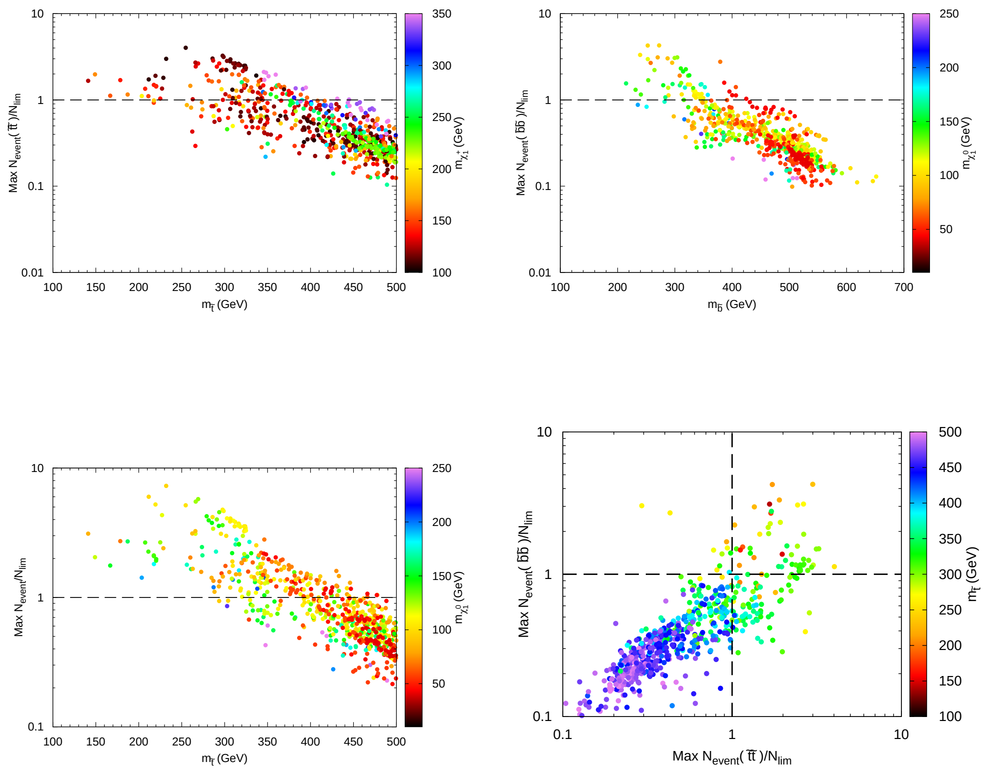

FIG. 17: Top left: the maximum value of $N(\tilde{t}\tilde{t}^*)/N_{lim}$ (which is determined by considering all $N(\tilde{t}\tilde{t}^*)/N_{lim}$ from different channels) versus stop mass, where the color scale indicates chargino mass. Top right: the maximum value of $N(\tilde{b}\tilde{b}^*)/N_{lim}$ versus sbottom mass, where the color scale indicates neutralino. Bottom left: the maximum value of $(N(\tilde{t}\tilde{t}^*)+N(\tilde{b}\tilde{b}^*))/N_{lim}$ versus stop mass, where the color scale indicates neutralino mass. Bottom right: the maximum value of $N(\tilde{b}\tilde{b}^*)/N_{lim}$ versus the maximum value of $N(\tilde{t}\tilde{t}^*)/N_{lim}$, where the color scale indicates stop mass.

Finally, it is should be mentioned that CMS and ATLAS collaboration have released a series of results of light stop/sbottom searches with 5 fb^{-1} of data [80–83]. Some results based on $\sqrt{s} = 8$ TeV have also been provided [79, 84]. In these searches, some powerful methods based on additional kinematic variables, such as "α_T" [80] and "*Razor*" [81], are performed. These analyses can set very stringent constraints on the sbottom and stop pair production with large $BR(\tilde{b} \to b\tilde{\chi}_1^0)$ and $BR(\tilde{t} \to t\tilde{\chi}_1^0)$. Some parameter points with $m_{\tilde{t}} > 500$ GeV may also be excluded. Here we do not perform these analyses, and leave them in the future studies.

C. benchmark points

Point	BMP1	BMP2	BMP3	BMP4
$\tan\beta$	5.84	11.8	16.7	3.66
λ	0.66	0.68	0.41	0.71
κ	0.18	0.34	0.47	0.16
μ (GeV)	183	152	223	221
A_λ (GeV)	1110	1742	2903	826
A_κ (GeV)	13.7	-2.83	-122	- 136
$A_t = A_b = A_\tau$ (GeV)	1370	1813	2233	-785
$M_{\tilde{Q}_3}$ (GeV)	556	514	1968	1189
$M_{\tilde{t}_R} = M_{\tilde{b}_R}$ (GeV)	998	1348	397	484
$M_{\tilde{\ell}_L} = M_{\tilde{\ell}_R}$ (GeV)	200	261	520	140
M_1 (GeV)	977	118	191	530
M_2 (GeV)	332	490	141	160

TABLE VII: Input parameters of four bench mark points.

In this subsection we choose four benchmark points that have passed all the constraints we considered above and discuss their features at the LHC. In Table .(VII) and Fig. (18), we tabulate the mass spectra as well as main decay modes of stop and sbottom of four benchmark points. In the first and fourth bench mark point, the SM-like Higgs boson is H_2; while in the second and third bench mark point, the SM-like Higgs boson is H_1. For all four bench mark points, the H_d dominated Higgs bosons, including H_3, A_2 and $H^\pm$ are quite heavy and are decoupled.

It is also noticed that the lightest stop and sbottom are left handed dominant in the first two bench mark points while are right-handed dominant in the other two bench mark points. Due to the branching fractions $BR(\tilde{t}_1 \to t\tilde{\chi}_1^0)$ of these bench mark points are less than 50% and also partially due to the mass splitting between $\delta m_{\tilde{t}} = m_{\tilde{t}_1} - m_{\tilde{\chi}_1^0}$, such four bench mark points have not been excluded by LHC searches.

There are some interesting phenomenologies for these benchmark points. It is noticed

Point	BMP1	BMP2	BMP3	BMP4
m_{H_1} (GeV)	108	125	125	84
m_{H_2} (GeV)	126	151	476	124
m_{A_1} (GeV)	85	100	290	180
$m_{\tilde{\chi}_1^0}$	78.5	66.7	118	80
$m_{\tilde{\chi}_2^0}$	211	135	182	163
$m_{\tilde{\chi}_1^\pm}$	165	149	125	124
$m_{\tilde{\chi}_2^\pm}$	370	516	267	274
$m_{\tilde{t}_1}$	497	475	346	462
$m_{\tilde{b}_1}$	534	504	402	474
$R(H_{SM} \to \gamma\gamma)$	1.17	1.29	1.01	1.23
$R(H_{SM} \to VV)$	1.11	1.20	0.98	1.16
$R(H_{SM} \to b\bar{b})$	0.89	0.83	1.00	0.91
$BR(\chi_1^\pm \to W^\pm \tilde{\chi}_1^0)$	100%	100%	(W^*) 100%	(W^*) 100%
$BR(\tilde{t}_1 \to t\tilde{\chi}_1^0)$	41.7%	38.7%	8.0%	22%
$BR(\tilde{t}_1 \to t\tilde{\chi}_2^0)$	9.9%	17.9%	-	-
$BR(\tilde{t}_1 \to t\tilde{\chi}_3^0)$	26.1%	32.8%	-	12.3%
$BR(\tilde{t}_1 \to t\tilde{\chi}_4^0)$	-	5.4%	-	1.9%
$BR(\tilde{t}_1 \to b\tilde{\chi}_1^+)$	1.8%	5.2 %	28.5%	30.0%
$BR(\tilde{t}_1 \to b\tilde{\chi}_2^+)$	20.4%	-	63.5%	34.3 %
$BR(\tilde{b}_1 \to b\tilde{\chi}_1^0)$	1.8%	2.8%	20.2%	10.4%
$BR(\tilde{b}_1 \to b\tilde{\chi}_2^0)$	3.5%	0.3%	33%	8.5 %
$BR(\tilde{b}_1 \to b\tilde{\chi}_3^0)$	0.7%	2.3%	19.0%	23.4%
$BR(\tilde{b}_1 \to b\tilde{\chi}_4^0)$	11.1%	1.3%	10.4%	20.7%
$BR(\tilde{b}_1 \to t\tilde{\chi}_1^-)$	82.9%	93.2%	17.2%	28.4%
$BR(\tilde{b}_1 \to t\tilde{\chi}_2^-)$	-	-	-	8.4%

TABLE VIII: Mass spectra as well as main decay modes of stop and sbottom in four bench mark points, where the label W^* in the row marked by $Br(\chi_1^\pm \to W^\pm \tilde{\chi}_1^0)$ means the off-shell W boson.

that the branching fraction of $\tilde{t}_1 \to t\tilde{\chi}_2^0$ and $\tilde{t}_1 \to t\tilde{\chi}_3^0$ can be quite large for the first two benchmark points. For the first benchmark point, the $\tilde{\chi}_2^0$ can dominantly decay to $H_2\tilde{\chi}_1^0$ with branching fraction 76.4%, then the signature $pp \to \tilde{t}_1\tilde{t}_1^* \to t\bar{t}H_2H_2\tilde{\chi}_1^0\tilde{\chi}_1^0$ can be sizable when luminosity is large enough. Therefore multi-bjets plus top pair searches should be useful for this channel. For the second benchmark point, the $\tilde{\chi}_2^0$ can dominantly decay to $\tilde{\chi}_1^0$ plus an off-shell Z boson with branching fraction 100%, then the signature $pp \to \tilde{t}_1\tilde{t}_1^* \to t\bar{t}Z^*Z^*\tilde{\chi}_1^0\tilde{\chi}_1^0$ (W^*, Z^* means off-shell gauge bosons) can be sizable when luminosity is large enough.

For the first benchmark point, the $\tilde{\chi}_3^0$ can dominantly decay to $Z(A_1)\chi_1^0$ with branching fraction 66.2% (31.3%), then the signature $pp \to \tilde{t}_1\tilde{t}_1^* \to t\bar{t}Z(A_1)Z(A_1)\tilde{\chi}_1^0\tilde{\chi}_1^0$ can be sizable. For the second benchmark point, the $\tilde{\chi}_3^0$ also goes to $Z(A_1)\tilde{\chi}_1^0$ but with branching fraction 83.0% (16.9%). Therefore, except the $pp \to t\bar{t}\tilde{\chi}_1^0\tilde{\chi}_1^0$ search, the search for $pp \to \tilde{t}_1\tilde{t}_1^* \to t\bar{t}Z(A_1)Z(A_1)\tilde{\chi}_1^0\tilde{\chi}_1^0$ can be complementary to constrain these two benchmark points (here the branching fraction of $A_1 \to b\bar{b}$ can be 90% for both benchmark points).

It is also remarkable that due to the fact that the lighter sbottom quarks are dominantly left-handed, consequently its dominant decay mode is $\tilde{b}_1 \to t\tilde{\chi}_1^-$ with branching fraction of 82.9% and 93.2% respectively. For both benchmark points the chargino $\tilde{\chi}_1^+$ decays 100% to $\tilde{\chi}_1^0$ and W boson. Therefore the production of $pp \to \tilde{t}_1\tilde{t}_1^*$ can leads to a sizable final state with $b\bar{b}W^+W^-W^+W^-\tilde{\chi}_1^0\tilde{\chi}_1^0$.

Obviously, the same sign lepton plus jets signature can help to constrain these two benchmark points. With more dataset accumulated at $\sqrt{s} = 8$ TeV [79], it is expected that the direct searches of LHC can either rule out or discover these three benchmark points.

For the third benchmark point, the decay mode $\tilde{t}_1 \to b\tilde{\chi}_2^+$ is quite large, while $\tilde{\chi}_2^+$ dominantly goes to $Z\tilde{\chi}_1^+$ and $W^+\tilde{\chi}_1^0$ with branching fraction 44.4% and 41.3%, respectively. Therefore the production of $pp \to \tilde{t}_1\tilde{t}_1^*$ can leads to sizable final states like $b\bar{b}W^+W^-\tilde{\chi}_1^0\tilde{\chi}_1^0$. The decay mode $\tilde{b}_1 \to b\tilde{\chi}_2^0$ is the dominated $\tilde{b}_1$ decay mode, while $\tilde{\chi}_2^0$ dominantly goes to $W^*\tilde{\chi}_1^-$.

For the forth benchmark points, more decay modes are open and many decay modes share large branching fractions. In the $\tilde{t}_1 \to b\tilde{\chi}_2^+$ mode, the heavier chargino $\tilde{\chi}_2^+$ dominantly goes to $H_2/H_1/Z\tilde{\chi}_1^+$ with branching fractions 36.0%/10.8%/14.7% and $W\tilde{\chi}_1^0/\tilde{\chi}_2^0$ with branching fractions 15.0%/10.5%. For the sbottom, the decay chains also become quite long. It might be more challenging to exclude or discover this benchmark point.

For comparison, we tested the benchmark point 3 given in [13] and found it is still alive.

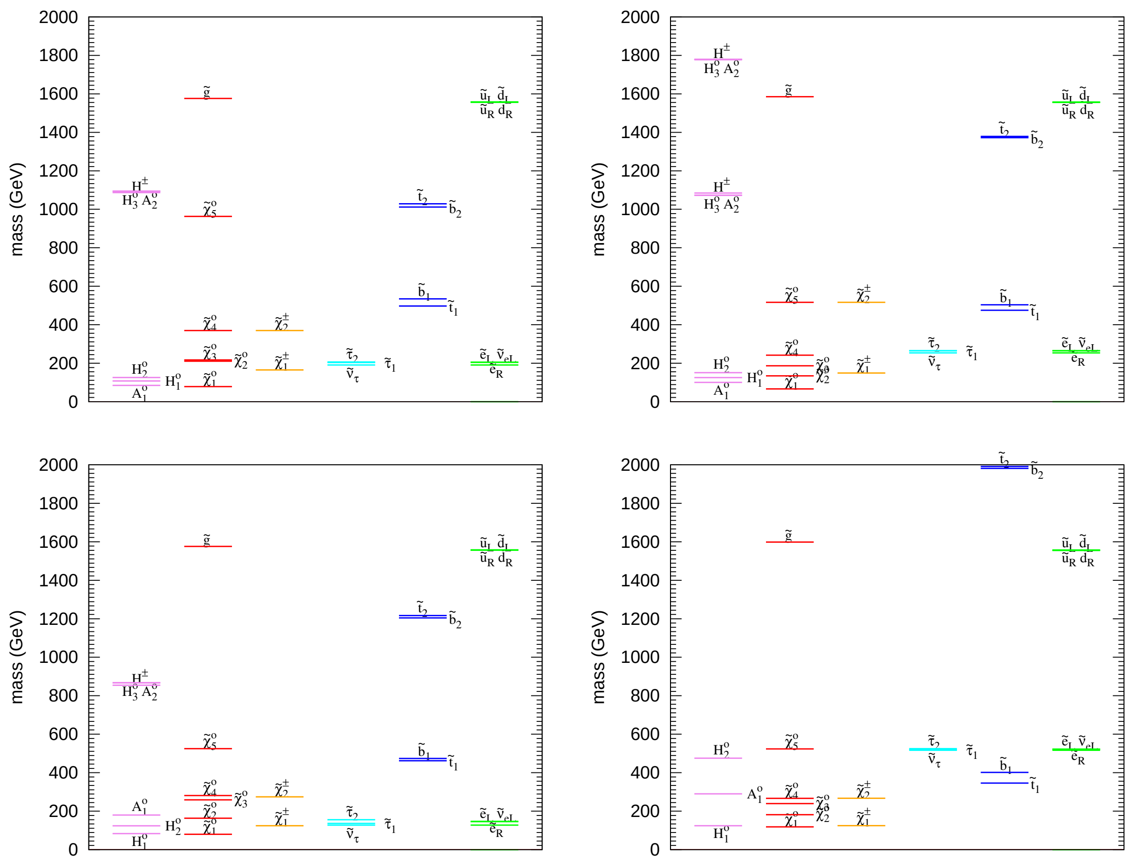

FIG. 18: Mass spectra of benchmark point 1 (top left), benchmark point 2 (top right), benchmark point 3 (bottom left), and benchmark point 4 (bottom right).

The main decay modes of light stop in this point are $\tilde{t}_1 \to t\tilde{\chi}_1^0$, $\tilde{t}_1 \to t\tilde{\chi}_2^0$ and $\tilde{t}_1 \to b\tilde{\chi}_2^+$ with branching fractions 16%, 29% and 45%, while $\tilde{\chi}_2^0$ and $\tilde{\chi}_2^+$ decay to $Z^*\tilde{\chi}_1^0$ and $Z/H_2\tilde{\chi}_1^+$ with large branching fractions respectively. We also tested the benchmark points given in [12] and found they can survived from the search of the direct LHC searches. The main decay modes of light stop in these two benchmark points are $\tilde{t}_1 \to t\tilde{\chi}_1^0$ and $\tilde{t}_1 \to b\tilde{\chi}_1^+$ with branching fractions 23% and 56% (20% and 68%). In these benchmark points, compared with the MSSM case, the branching fractions of $\tilde{b}_1 \to b\tilde{\chi}_1^0$ and $\tilde{t}_1 \to t\tilde{\chi}_1^0$ can be suppressed drastically if $\tilde{\chi}_1^0$ is singlino dominant. Such a fact leads to weaker constraints when we apply the LHC direst searches to parameter spaces with lighter stop and sbottom.

IV. CONCLUSIONS

The NMSSM provides a natural framework for the recently discovered 125 GeV Higgs boson. Within the NMSSM, we have analyzed the constraints from the 125 GeV Higgs boson as well as the results from the dark matter searches to the parameter space. We concentrate on the LHC direct SUSY searches on the allowed parameter points.

We have focused on scenario where the stop/sbottom can be lighter than 500 GeV and performed a detailed study to examine how the SUSY direct search can constrain them by using the results based on $\sqrt{s}$ =7 TeV and $2 \sim 5$ fb^{-1} of data. It is found that the direct SUSY searches, especially the channels with tagged b jets, are powerful and can put bounds to the allowed parameter space.

We would like to point out that when the inclusive signatures of both stop and sbottom pair productions are considered, the direct SUSY searches can exclude many parameter points with the left-handed stop/sbottom up to 500 GeV or so. With $\sqrt{s}$ =8 TeV and 5 fb^{-1} of data or more, although kinematics could be a little different, we can expect the direct SUSY searches will push the light third generation squarks of NMSSM to narrower corners. However, for benchmark points given in our work and Ref. [12, 13], special strategies and kinematic variables are still needed for searching light stop/sbottom pair signatures.

Acknowledgments

The authors thank Tianjun Li and Jinmin Yang for valuable comments on the manuscript. The authors also thank Zhao-huan Yu for helpful discussions. This work is supported by the Natural Science Foundation of China under the grant NO. 11105157, NO. 11075169 and No. 11175251, the 973 project under grant No. 2010CB833000, and the Chinese Academy of Science under Grant No. KJCX2-EW-W01.

---

[1] G. Aad *et al.* [ATLAS Collaboration], arXiv:1207.7214 [hep-ex].

[2] S. Chatrchyan *et al.* [CMS Collaboration], arXiv:1207.7235 [hep-ex].

[3] T. Aaltonen *et al.* [CDF Collaboration], arXiv:1207.1707 [hep-ex].

[4] V. M. Abazov *et al.* [D0 Collaboration], arXiv:1207.6631 [hep-ex].

[5] R. Kitano and Y. Nomura, Phys. Rev. D **73**, 095004 (2006) [hep-ph/0602096].

[6] M. Papucci, J. T. Ruderman and A. Weiler, arXiv:1110.6926 [hep-ph].

[7] J. F. Gunion, Y. Jiang and S. Kraml, Phys. Lett. B **710**, 454 (2012) [arXiv:1201.0982 [hep-ph]].

[8] M. Carena, S. Gori, N. R. Shah and C. E. M. Wagner, JHEP **1203**, 014 (2012) [arXiv:1112.3336 [hep-ph]].

[9] K. Cheung and T. -C. Yuan, Phys. Rev. Lett. **108**, 141602 (2012) [arXiv:1112.4146 [hep-ph]].

[10] D. Carmi, A. Falkowski, E. Kuflik, T. Volansky and J. Zupan, arXiv:1207.1718 [hep-ph].

[11] U. Ellwanger, JHEP **1203**, 044 (2012) [arXiv:1112.3548 [hep-ph]].

[12] U. Ellwanger and C. Hugonie, arXiv:1203.5048 [hep-ph].

[13] S. F. King, M. Muhlleitner and R. Nevzorov, Nucl. Phys. B **860**, 207 (2012) [arXiv:1201.2671 [hep-ph]].

[14] K. Schmidt-Hoberg and F. Staub, arXiv:1208.1683 [hep-ph].

[15] A. Djouadi, V. Driesen, W. Hollik and J. I. Illana, Eur. Phys. J. C **1**, 149 (1998) [hep-ph/9612362].

[16] J. -J. Cao, Z. -X. Heng, J. M. Yang, Y. -M. Zhang and J. -Y. Zhu, JHEP **1203**, 086 (2012) [arXiv:1202.5821 [hep-ph]].

[17] M. Carena, S. Gori, N. R. Shah, C. E. M. Wagner and L. -T. Wang, JHEP **1207**, 175 (2012) [arXiv:1205.5842 [hep-ph]].

[18] K. Blum, R. T. D'Agnolo and J. Fan, arXiv:1206.5303 [hep-ph].

[19] R. Benbrik, M. G. Bock, S. Heinemeyer, O. Stal, G. Weiglein and L. Zeune, arXiv:1207.1096 [hep-ph].

[20] Z. Kang, T. Li, J. Li and Y. Liu, arXiv:1208.2673 [hep-ph].

[21] A. Fowlie, A. Kalinowski, M. Kazana, L. Roszkowski and Y. L. S. Tsai, Phys. Rev. D **85**, 075012 (2012) [arXiv:1111.6098 [hep-ph]].

[22] S. Sekmen, S. Kraml, J. Lykken, F. Moortgat, S. Padhi, L. Pape, M. Pierini and H. B. Prosper *et al.*, JHEP **1202**, 075 (2012) [arXiv:1109.5119 [hep-ph]].

[23] G. Aad *et al.* [ATLAS Collaboration], arXiv:1208.0949 [hep-ex].

[24] S. Chatrchyan *et al.* [CMS Collaboration], arXiv:1207.1898 [hep-ex].

[25] X. -J. Bi, Q. -S. Yan and P. -F. Yin, Phys. Rev. D **85**, 035005 (2012) [arXiv:1111.2250 [hep-ph]].

[26] N. Desai and B. Mukhopadhyaya, JHEP **1205**, 057 (2012) [arXiv:1111.2830 [hep-ph]].

[27] M. A. Ajaib, T. Li and Q. Shafi, Phys. Rev. D **85**, 055021 (2012) [arXiv:1111.4467 [hep-ph]].

[28] M. Drees, M. Hanussek and J. S. Kim, arXiv:1201.5714 [hep-ph].

[29] Y. Bai, H. -C. Cheng, J. Gallicchio and J. Gu, arXiv:1203.4813 [hep-ph].

[30] Z. Han, A. Katz, D. Krohn and M. Reece, arXiv:1205.5808 [hep-ph].

[31] T. Plehn, M. Spannowsky and M. Takeuchi, arXiv:1205.2696 [hep-ph].

[32] D. E. Kaplan, K. Rehermann and D. Stolarski, JHEP **1207**, 119 (2012) [arXiv:1205.5816 [hep-ph]].

[33] D. S. M. Alves, M. R. Buckley, P. J. Fox, J. D. Lykken and C. -T. Yu, arXiv:1205.5805 [hep-ph].

[34] C. Brust, A. Katz and R. Sundrum, [arXiv:1206.2353 [hep-ph]].

[35] J. Cao, C. Han, L. Wu, J. M. Yang and Y. Zhang, arXiv:1206.3865 [hep-ph].

[36] J. Bramante, J. Kumar and B. Thomas, Phys. Rev. D **86**, 015014 (2012) [arXiv:1109.6014 [hep-ph]].

[37] M. Adeel Ajaib, T. Li and Q. Shafi, Phys. Lett. B **701**, 255 (2011) [arXiv:1104.0251 [hep-ph]].

[38] E. Alvarez and Y. Bai, arXiv:1204.5182 [hep-ph].

[39] H. M. Lee, V. Sanz and M. Trott, JHEP **1205**, 139 (2012) [arXiv:1204.0802 [hep-ph]].

[40] U. Ellwanger, C. Hugonie and A. M. Teixeira, Phys. Rept. **496**, 1 (2010) [arXiv:0910.1785 [hep-ph]].

[41] U. Ellwanger, J. F. Gunion and C. Hugonie, JHEP **0502**, 066 (2005) [hep-ph/0406215]; U. Ellwanger and C. Hugonie, Comput. Phys. Commun. **175**, 290 (2006) [hep-ph/0508022].

[42] S. Dimopoulos, G. F. Giudice, Phys. Lett. **B357**, 573-578 (1995) [hep-ph/9507282]; A. Pomarol, D. Tommasini, Nucl. Phys. **B466**, 3-24 (1996) [hep-ph/9507462]; A. G. Cohen, D. B. Kaplan, A. E. Nelson, Phys. Lett. **B388**, 588-598 (1996) [hep-ph/9607394]; V. D. Barger, C. Kao, R. -J. Zhang, Phys. Lett. **B483**, 184-190 (2000) [hep-ph/9911510].

[43] E. Barberio *et al.* [Heavy Flavor Averaging Group (HFAG) Collaboration], hep-ex/0603003.

[44] D. Asner *et al.* [Heavy Flavor Averaging Group Collaboration], arXiv:1010.1589 [hep-ex].

[45] A. Abulencia *et al.* [CDF Collaboration], Phys. Rev. Lett. **97**, 242003 (2006) [hep-ex/0609040].

[46] G. Aad *et al.* [ATLAS Collaboration], Phys. Lett. B **713**, 387 (2012) [arXiv:1204.0735 [hep-ex]].

[47] S. Chatrchyan *et al.* [CMS Collaboration], JHEP **1204**, 033 (2012) [arXiv:1203.3976 [hep-ex]].

[48] R. Aaij *et al.* [LHCb Collaboration], Phys. Rev. Lett. **108**, 231801 (2012) [arXiv:1203.4493

[hep-ex]].

[49] D. Larson *et al.*, Astrophys. J. Suppl. **192**, 16 (2011) [arXiv:1001.4635 [astro-ph.CO]].

[50] G. Belanger, F. Boudjema, A. Pukhov and A. Semenov, Comput. Phys. Commun. **176** (2007) 367 [arXiv:hep-ph/0607059]; arXiv:0803.2360 [hep-ph]; arXiv:1005.4133 [hep-ph].

[51] D. A. Vasquez, G. Belanger, C. Boehm, A. Pukhov and J. Silk, Phys. Rev. D **82**, 115027 (2010) [arXiv:1009.4380 [hep-ph]].

[52] J. Cao, Z. Heng, J. M. Yang and J. Zhu, JHEP **1206**, 145 (2012) [arXiv:1203.0694 [hep-ph]].

[53] D. A. Vasquez, G. Belanger, C. Boehm, J. Da Silva, P. Richardson and C. Wymant, arXiv:1203.3446 [hep-ph].

[54] J. Baglio, A. Djouadi and R. M. Godbole, arXiv:1207.1451 [hep-ph].

[55] D. Albornoz Vasquez, G. Belanger and C. Boehm, Phys. Rev. D **84**, 095008 (2011) [arXiv:1107.1614 [hep-ph]].

[56] M. Ackermann *et al.* [Fermi-LAT Collaboration], Phys. Rev. Lett. **107**, 241302 (2011) [arXiv:1108.3546 [astro-ph.HE]].

[57] E. Aprile *et al.* [XENON100 Collaboration], arXiv:1104.2549 [astro-ph.CO].

[58] E. Aprile *et al.* [XENON100 Collaboration], arXiv:1207.5988 [astro-ph.CO].

[59] E. Behnke, J. Behnke, S. J. Brice, D. Broemmelsiek, J. I. Collar, P. S. Cooper, M. Crisler and C. E. Dahl *et al.*, Phys. Rev. Lett. **106**, 021303 (2011) [arXiv:1008.3518 [astro-ph.CO]].

[60] H. S. Lee *et al.* [KIMS Collaboration], Phys. Rev. Lett. **99**, 091301 (2007) [arXiv:0704.0423 [astro-ph]].

[61] T. Tanaka *et al.* [Super-Kamiokande Collaboration], Astrophys. J. **742**, 78 (2011) [arXiv:1108.3384 [astro-ph.HE]].

[62] R. Abbasi *et al.* [IceCube Collaboration], Phys. Rev. D **85**, 042002 (2012) [arXiv:1112.1840 [astro-ph.HE]].

[63] W. Beenakker, R. Hopker and M. Spira, arXiv:hep-ph/9611232.

[64] M. Maniatis and Y. Schroder, arXiv:1207.0729 [hep-ph].

[65] J. Alwall, M. Herquet, F. Maltoni, O. Mattelaer and T. Stelzer, JHEP **1106**, 128 (2011) [arXiv:1106.0522 [hep-ph]].

[66] T. Sjostrand, S. Mrenna and P. Z. Skands, JHEP **0605**, 026 (2006) [arXiv:hep-ph/0603175].

[67] PGS-4, J. Conway et al. conway/research/software/pgs/pgs4-general.htm

[68] G. Aad *et al.* [ATLAS Collaboration], arXiv:1109.6572 [hep-ex].

[69] P. J. Fox, R. Harnik, J. Kopp and Y. Tsai, Phys. Rev. D **85**, 056011 (2012) [arXiv:1109.4398 [hep-ph]].

[70] M. Carena, A. Freitas and C. E. M. Wagner, JHEP **0810**, 109 (2008) [arXiv:0808.2298 [hep-ph]].

[71] S. Chatrchyan *et al.* [CMS Collaboration], arXiv:1206.5663 [hep-ex].

[72] H. Baer, V. Barger, P. Huang and X. Tata, JHEP **1205**, 109 (2012) [arXiv:1203.5539 [hep-ph]].

[73] G. Aad *et al.* [ATLAS Collaboration], Phys. Rev. Lett. **108** (2012) 181802 [arXiv:1112.3832 [hep-ex]].

[74] D. R. Tovey, JHEP **0804**, 034 (2008) [arXiv:0802.2879 [hep-ph]].

[75] G. Aad *et al.* [ATLAS Collaboration], Phys. Rev. D **85**, 112006 (2012) [arXiv:1203.6193 [hep-ex]].

[76] The CMS collaboration, PAS-SUS-11-003, http://cdsweb.cern.ch/record/1459810

[77] G. Aad *et al.* [ATLAS Collaboration], arXiv:1208.2590 [hep-ex].

[78] G. Aad *et al.* [ATLAS Collaboration], arXiv:1208.1447 [hep-ex].

[79] The ATLAS collaboration, CONF-2012-105, http://cdsweb.cern.ch/record/1472674

[80] The CMS collaboration, PAS-SUS-11-022, https://cdsweb.cern.ch/record/1461947

[81] The CMS collaboration, PAS-SUS-11-024, http://cdsweb.cern.ch/record/1459813

[82] The ATLAS collaboration, CONF-2012-106, http://cdsweb.cern.ch/record/1472685

[83] G. Aad *et al.* [ATLAS Collaboration], arXiv:1208.4305 [hep-ex].

[84] The CMS collaboration, PAS-SUS-12-016, https://cdsweb.cern.ch/record/1460095